Acoustofluidics at Audible Frequencies-A review

Chuanyu Zhang, Philippe Brunet, Shuo Liu, Xiaofeng Guo, Laurent Royon, Xianming Qin, Xueyong Wei

Journal Pre-proofs

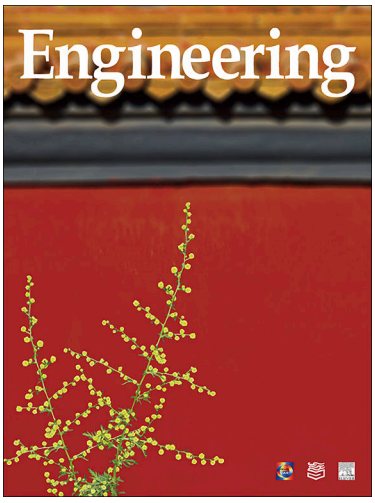

Review

Acoustofluidics at Audible Frequencies—A review

Chuanyu Zhang, Philippe Brunet, Shuo Liu, Xiaofeng Guo, Laurent Royon, Xianming Qin, Xueyong Wei

PII: S2095-8099(24)00321-7
DOI: https://doi.org/10.1016/j.eng.2024.03.020
Reference: ENG 1580

To appear in: *Engineering*

Received Date: 18 July 2023
Revised Date: 20 February 2024
Accepted Date: 13 March 2024

Please cite this article as: C. Zhang, P. Brunet, S. Liu, X. Guo, L. Royon, X. Qin, X. Wei, Acoustofluidics at Audible Frequencies—A review, *Engineering* (2024), doi: https://doi.org/10.1016/j.eng.2024.03.020

Research

Mechanical Engineering—Review

Acoustofluidics at Audible Frequencies—A review

Chuanyu Zhang [a,b], Philippe Brunet [c,*], Shuo Liu [b,d], Xiaofeng Guo [e], Laurent Royon [e], Xianming Qin [f], Xueyong Wei [a,b,*]

[a] *School of Instrument Science and Technology, Xi'an Jiaotong University, Xi'an 710049, Shannxi, China*

[b] *State Key Laboratory for Manufacturing Systems Engineering, Xi'an Jiaotong University, Xi'an 710049, Shannxi, China*

[c] *Laboratoire Matiére et Systémes Complexes, Université Paris Cité, UMR 7057 CNRS Paris 75013 France*

[d] *School of Mechanical Engineering, Xi'an Jiaotong University, Xi'an 710049, Shannxi, China*

[e] *Laboratoire Interdisciplinaire des Energies de Demain, Université Paris Cité, UMR 8236, CNRS, Paris 75013, France*

[f] *School of Mechano-Electronic Engineering, Xidian University, Xi'an 710071, Shannxi China*

* Corresponding authors.

E-mail addresses: philippe.brunet@univ-paris-diderot.fr (P. Brunet); seanwei@mail.xjtu.edu.cn (X. Wei);

Abstract: Acoustofluidics is a term describing the class of phenomena in which mechanical or acoustic vibrations induce a deformation or a flow in a fluid. Many deficiencies in our understanding of these phenomena remain to be addressed, with respect to the fundamental theoretical framework as well as in numerous applications. In this regard, the frequency of external forcing is a key parameter. Owing to the low cost, substantial magnitude, and versatility associated with acoustofluidic phenomena at audible frequencies, studies of these phenomena in the audible range have emerged with increasing amount in recent years and have attracted considerable attention. However, compared with studies focusing on the ultrasonic frequency domain, critical features and information specific to audible acoustofluidics remain dispersed across many independent publications, and a systematic integration of the literature on this topic is necessary. Accordingly, this review summarizes the basic theory and methods for generating vibrations in the audible range, presents various applications thereof in biology, chemistry, and other fields, and provides a high-level overview of the current status of the topic to motivate developing interesting proposals for further research in this field of study.

Keywords: Acoustofluidics; Audible frequency; Vibration generation; Biological detection; Particle manipulation; Mixing; Chemical reaction; Micropumping; Heat transfer

1. Introduction

Acoustofluidics, which is concerned with the actuation of fluids by mechanical or acoustic vibrations, is characterized by complex processes attending the transfer of acoustic energy (carried by a standing or propagative wave) to hydrodynamic energy (carried by a fluid flow, a deformation of a free fluid surface, or the motion or trapping of particles in a fluid). Acoustofluidics encompasses a variety of phenomena that are being revealed in an increasing number of studies. Notably, the mechanisms inherent in acoustofluidics enable the active manipulation of fluids or solid particles at scales ranging from a few meters (for example, in Kundt's tubes [1]) to a few microns (as in the trapping of microparticles [2]). The fluid flow generated above a vibrating plate was first studied by

Faraday [3] approximately 200 years ago. Such actuation of fluids at a macroscopic scale has attracted much attention in studies of acoustics as well as studies of fluid mechanics. Nyborg [4,5] proposed a theoretical framework for acoustic streaming near boundaries (denoted as Rayleigh–Schlichting streaming), followed by Lighthill [6], who provided a complementary and comprehensive research framework, presenting the streaming flow as originating from the Reynolds stress. For decades, acoustofluidic phenomena have been mainly investigated in terms of fundamental questions, with notable exceptions such as the study by Trinh and Gopinath [7], who developed a convection enhancement process in a microgravity environment with ultrasonic levitators. In 1995, Johnson and Feke [8] and Yasuda et al. [2] used ultrasonic standing waves to concentrate and break particle suspensions in fluids. Those studies opened a new field of research by highlighting the considerable potential of acoustofluidics for manipulating biosuspensions, especially in microfluidics. Being mostly biocompatible, contactless, and, in some situations, cost-effective, acoustofluidics has stimulated further studies owing to its potential benefits in the fields of microfluidics and nanofluidics. This has led to the concept of the laboratory-on-a-chip, where flows are dominated by viscosity. At present, fundamental aspects of the field have matured to a level where applications may now approach optimal conditions. In recent decades, studies based on acoustofluidics and acoustophoresis have rapidly increased in number, and substantial progress in the applications of these techniques has been achieved.

1.1. Classification of acoustofluidic phenomena

The related parameters to the acoustofluidics are included in Table1. The frequency (f) is the key parameter associated with actuating vibration and it occupies a central role in all acoustofluidic phenomena. Fig. 1 [9–21] shows various phenomena occurring across a frequency spectrum ranging from less than 1 Hz to more than 1 GHz, where the lowest frequencies correspond to the formation of a rippled surface on a sandy seabed [9,22] and the highest frequencies are associated with the control of particles at a submicron scale in blood samples [21,23]. The different examples shown in this figure emphasize the universality shared by the phenomena. This is a counter-intuitive observation, given the considerable range of frequencies covered. For example, the streaming flows around immersed objects vibrating at a few tens of hertz are similar in appearance to those around bubbles excited at several tens of kilohertz. Historically, Kundt's tube, originally designed by August Kundt in 1866 [1], was a model experiment composed of a loudspeaker connected to a hollow tube where standing acoustic waves (generally prescribed at an audible frequency) could be visualized by their action on dust or other particles filling the tube [24,25]. At higher frequencies and shorter wavelengths, the scale of the interactions between the wave and fluid decreases from meters to micro- or nanometers. From the perspective of classes of phenomena, acoustofluidics at frequencies below 20 kHz mainly involve streaming flow near boundaries (Rayleigh–Schlichting streaming), but not the bulk counterpart thereof (Eckart streaming or quartz wind), because of the negligible attenuation of the wave.

At frequencies ranging from several hertz to hundreds of hertz, streaming flows can be generated near vibrating rods and beams [10,26–35], as shown in Fig. 1(b). The flow results from the generation of vorticity within the viscous boundary layer (VBL) around the vibrating body, which, in turn, can generate outer vortices at a larger distance. In addition, directional synthetic jets can be generated by periodic flow or vibrations near orifices [36–38] and have found promising applications in the control of aerodynamic flows [39].

One of the major advantages of streaming flows in pumping or mixing applications is that they are (supposedly) independent of fluid viscosity, validating them as potential vehicles for handling viscous fluids. This counterintuitive feature originates from the fact that viscosity is involved in both the generation and the damping of a flow. The viscosity independence of streaming flows has been found to hold subject to the condition that the scale of the flow is sufficiently small compared with the size of the system [33].

When a free surface is involved, propagative surface waves can induce directional mass transport, which originates from a phenomenon similar to steady streaming [40]. Immersed transducers shooting up to the free surface can generate acoustic fountains, where a bulge can be observed

together with a mist of droplets [41,42]. More recently, it has been observed that the slanted vibrations of a substrate can induce the directional motion of droplets, with the direction and velocity strongly dependent on frequency [43,44]. At higher amplitudes and over a larger frequency range, the atomization of sessile droplets could be induced at frequencies of a few hundred hertz to 1 kHz [13]. Several modes of surface waves appeared on the sessile droplet, and the increase in the vibration amplitude could generate the breakup of the interface and subsequent ejection of smaller droplets.

When the frequency is slightly higher, with a piezoelectric transducer (PZT) disk attached to the substrate and vibrating at a few kilohertz, an intense streaming flow can be excited near sharp-edge structures [45–47], where the local geometrical scale (namely, the radius of curvature of the structure) is comparable with or smaller than the thickness of the VBL.

In addition to acoustic streaming, sound waves can induce a radiation force acting at the interfaces between media of different acoustic impedances. This force can trap solid particles suspended in a fluid [47–49] or deform the free surfaces between two fluids [41,42]. Associated applications consist of particles clustering in microfluidic devices or being sorted, depending on the specific particle properties (size or acoustic index). This form of radiation pressure was first detected experimentally by Ernst Chladni [50]. The familiar Chladni patterns can be observed when sand or dust is shaken on a vibrating surface at a frequency ranging from hundreds to thousands of hertz, as shown in Fig. 1(d) [12]. Its general principle relies on generating a standing pressure field that enables the micro- or nanoparticles to move between the pressure nodes and antinodes. For traveling waves, a significant pressure gradient forms along the traveling direction. As shown in Fig. 1(l), in the study of Qin et al. [20], a droplet was trapped by superimposed traveling and standing waves at the crossover point. The generation of standing waves in sub-millimeter geometries implies that the typical frequency is equal to or higher than a few megahertz, given the velocity of sound in water. Therefore, except in the specific case of Chladni patterns in air, the radiation pressure in most acoustofluidic phenomena is only significant at frequencies considerably higher than 20 kHz, which falls outside the audible frequency range. Consequently, this review focuses predominantly on phenomena related to acoustic streaming.

Table 1

Definition of main physical quantities and abbreviations

Alternating current	AC
Sound velocity	c_s
Liquid density	ρ
Circulating tumor cells	CTC
Characteristic length, channel length	L
Enzyme-linked immunosorbent assays	ELISA
Forcing amplitude	A
Wave/Forcing frequency, angular frequency, period	f, ω, T

Kinematic viscosity	ν
Keuleghan–Carpenter number	KC
Mach number	Ma
Minnaert frequency	f_M
Navier–Stokes	N–S
Oscillating, steady pressure, and its amplitude	p_ω,p_s,p_a
Perturbation theory	PT
Point-of-care test	POCT
Piezoelectric transducer	PZT
Perfectly matched layer	PML
Surface acoustic wave	SAW
Size of the vibrating object	d
Viscous boundary layer	VBL
Viscous boundary layer thickness	δ
Tip radius of curvature	r_c
Tip angle of sharp edge	α
Wavelength	λ
Limit velocity method	LVM
Amplitude of vibration velocity	v_a

Reynolds number	Re
Bubble radius	r_b
Streaming velocity, its maximum value	v_s, $v_{s,max}$
Slip velocity	v_l
Stokes number	β
Width and Length of the channel	w, L
Womersley number	Wo

1.2. Why focus on phenomena at audible frequencies?

Although acoustofluidics conducted at ultrasonic frequencies has proven its accuracy and high resolution in addressing many of the requirements of microfluidics, several inherent challenges remain. Acoustic cavitation may occur as the vibration is driven to a relatively high intensity, resulting in potentially destructive effects and considerable thermal side effects, which must be avoided, especially when biosamples are concerned.

The relatively high cost of fabrication of microchips remains a detrimental factor in the application of acoustofluidics. In recent decades, the strengths and weaknesses associated with the application of acoustofluidics have been summarized and discussed in various studies, such as the serial reviews edited by Bruus et al. [51]. These studies comprised systematic analyses from various perspectives, such as the theoretical basis and applications of acoustofluidics. Reviews by Friend and Yeo [49] presented a state-of-the-art account of acoustofluidics, with a particular focus on microfluidics, as well as on specific features of surface acoustic waves (SAWs). Other notable studies by various authors [47,48,52,53] respectively presented the application of SAWs , acoustic tweezers, and cell separation. All these studies were concerned with theories and applications related to acoustofluidics, but the majority of them were concentrated on phenomena occurring at ultrasonic frequencies. However, acoustofluidics applied at audible (or lower) frequencies offers specific advantages in both the fundamental and applied contexts.

Various other studies opted for liquid actuation within the audible range because of its multiple advantages, the first of which is the possibility of using versatile and cost-effective actuators and amplifiers for broadband operations with a relatively well-controlled forcing. Furthermore, audible-range actuators allow the use of vibrations with relatively high amplitudes at reasonable power levels. As elucidated in Section 2 of this paper, the typical streaming velocity can reach sufficiently high values for more complex flows or behaviors to occur. This approach is justified on theoretical grounds, specifically through the estimation of relevant dimensionless numbers.

Therefore, the present review aims to encapsulate the specific features of acoustofluidics at frequencies below the ultrasonic range, typically between 1 and 20 kHz, and to present fundamental questions specific to this range. We also present current achievements in terms of applications and anticipated future outcomes in the audible range.

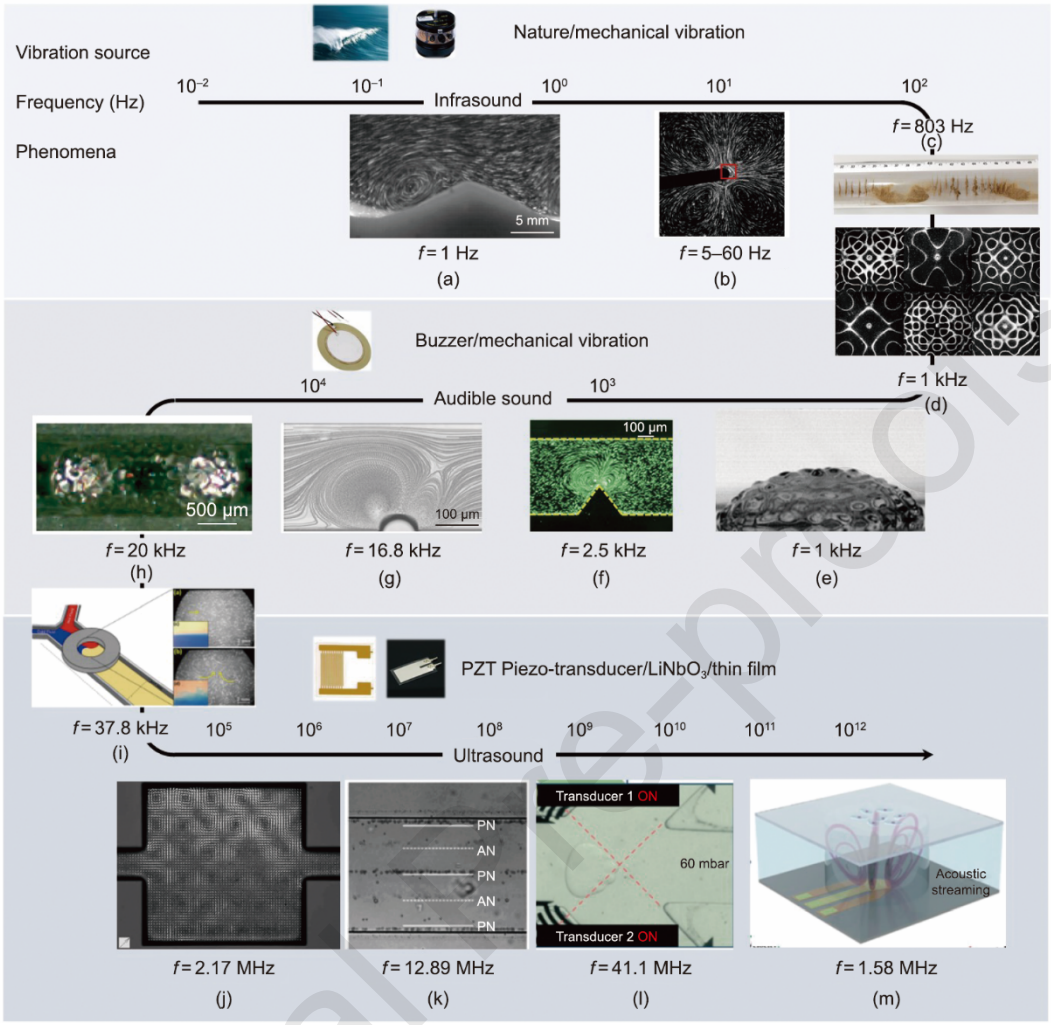

Fig. 1. Acoustofluidics situations across a wide range of actuation frequencies, from less than 1 Hz to beyond 1 GHz. Such as: (a) formation of a rippled surface on a sandy seabed, reproduced from Ref. [9] with permission; (b) symmetrical vortices formed near vibrating rod, reproduced from Ref. [10] with permission; (c) accumulation of powder at the nodes of the standing wave inside the Kundt's tube, image reproduced from Ref. [11] with permission; (d) Chladni Plates, image reproduced from Ref. [12] with permission; (e) a sessile drop in forced vibration, reproduced from Ref. [13] with permission; (f) acoustic streaming near a sharp structure, reproduced from Ref. [14] with permission; (g) acoustic streaming near a bubble, reproduced from Ref. [15] with permission; (h) cavitation effect in a ultrasonic microreactor, reproduced from Ref. [16] with permission; (i) mixing enhanced by streaming flow under an actuator, reproduced from Ref. [17] with permission; (j) streaming flow in a resonant chamber, reproduced from Ref. [18] with permission; (k) cells pattern by acoustic radiation force, reproduced from Ref. [19]; (l) acoustic valve effect for a droplet, reproduced from Ref. [20] with permission; (m) streaming flow induced at GHz, reproduced from Ref. [21] with permission.

2. Basics of acoustofluidics phenomena at audible frequencies

2.1. Typical examples of flows

In the various examples shown in Fig. 1, the streaming flows appear as one or several vortices near the boundaries. At audible frequencies, the majority of the streaming flows are of the Rayleigh–Schlichting type, which is associated with the generation of vorticity in the VBL, owing to the dissipation and relatively large shear stress induced by the no-slip boundary condition. In such situations, the streaming flow structure is closely related to the shape of the solid boundary. In a Kundt's tube [1,24,25], an array of vortices appears with a spatial periodicity equal to half the sound wavelength, $\frac{\lambda}{2}$ (see the sketch in Fig. 2(a) [54]). In the scenario of an immersed vibrating cylinder

or beam [10,26–34], streaming takes the form of four inner streaming vortices within the VBL around the cylinder and outer streaming vortices of a typical size equal to the rod diameter. Stuart [28] interpreted this type of streaming flow as a double-layer structure, where the inner streaming is confined within the Stokes layer (acoustic boundary layer), and the outer stream is driven by the boundary of the inner vortices. Vorticity is created in the inner region and convected away from the immersed object. Quantitative flow measurements generally show that the typical streaming velocity v_s (often taken as the maximal value of velocity along the axis of vibration) scales as $v_s \sim \frac{A^2 f}{d}$, with d being the typical object size, hence confirming the independence of viscosity invoked earlier, A . In Fig. 2(b), we show how Bahrani et al. [10] experimentally captured this classical double layer in a streaming flow and demonstrated that, at a sufficiently large amplitude, the outer vortices stretch along the vibration axis. In all these studies, the thickness of the inner region was found to be comparable to that of the unsteady boundary layer, expressed as follows:

$$\delta = \sqrt{\frac{\nu}{\pi f}} \quad (1)$$

Thus, at relatively high frequencies (typically several tens of kilohertz and up to several megahertz), the inner layer is too thin to be captured by visualization in an experiment, at least for liquids with viscosities comparable to that of water. For bubble or solid boundaries, the momentum of streaming originates near the interfaces and is dissipated by the viscosity in regions away from these boundaries.

Depending on the geometry of the boundary walls, the streaming flow can appear as a strongly directional jet. Fig. 2(c) shows the velocity field generated by the flow vibrations around a sharp structure on the channel wall [14]. In a similar geometry but under different conditions, the flow can present a more classical structure with two inner vortices bounded by larger and weaker outer vortices (Fig. 2(d)), as well as an unexpected asymmetric field (Fig. 2(e) [55]).

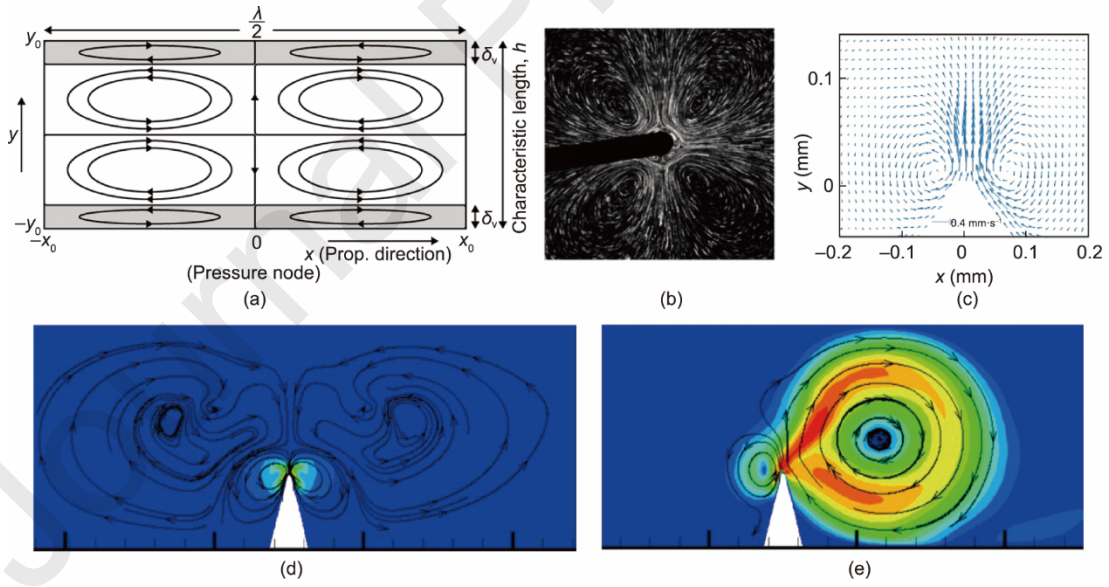

Fig. 2. Some examples of boundary-layer driven streaming flows in classical geometry. (a) Sketch of inner and outer streaming vortices at ultrasonic frequency in the presence of smooth walls. Reproduced from Ref. [54] with permission. (b) Experimental visualization of inner and outer regions of streaming flow generated by an immersed beam vibrating at a f between 5 and 100 Hz. Reproduced from Ref. [10] with permission. (c) Streaming velocity field near a sharp edge, generated by a longitudinal periodic forcing. Reproduced from Ref. [14] with permission. (d, e) Sharp-edge channel geometry similar to (c) with a transition of the streaming flow from a (d) symmetric to an (e) asymmetric flow, induced by an increase of the forcing amplitude (f = 10 Hz for both cases); (d) v_a = 0.02 mm·s^{-1} and $A \simeq 0.318$ mm ; and (e) v_a = 0.05 mm·s^{-1} and $A \simeq 0.796$ mm. Reproduced from Ref. [55] with permission.

2.2. Excitation of low-frequency vibrations for acoustofluidics

2.2.1. Vibration source

As shown in Fig. 3, electromechanical shakers, loudspeakers, and PZTs are commonly used to generate vibrations in the audible frequency range. Shakers can be relatively expensive and require dedicated high-fidelity amplifiers to achieve rectilinear high-amplitude forcing across a wide range of audible or infrasound frequencies. Mechanical coupling with fluids is generally ensured by solid walls or immersed objects connected to a shaker. Loudspeakers can be used as less expensive alternatives to shakers, but are less adapted to direct contact with liquids. Instead, they have been widely used in fundamental studies of acoustic streaming in air, such as in Kundt's tubes [24,25]. Piezoelectric (PZT) buzzers are commonly used in cost-effective applications at a very low cost per unit. Furthermore, they do not require expensive amplifiers to deliver relatively powerful waves. This suggests that audible frequency forcing in acoustofluidics may be achieved with cost-effective equipment. As shown in Fig. 3, a PZT disk consists of two layers: the PZT material at the top and a copper (or any other conductive metal) layer at the bottom. As an AC voltage is prescribed on both sides of the PZT material, the entire disk vibrates at several resonance frequencies, generally ranging between a few hundred hertz and several hundred kilohertz, and the acoustic power can be controlled by adjusting the peak-to-peak voltage. The classical excitement parameters of previous studies have been included in Table 2 [10,14,34,56–64].

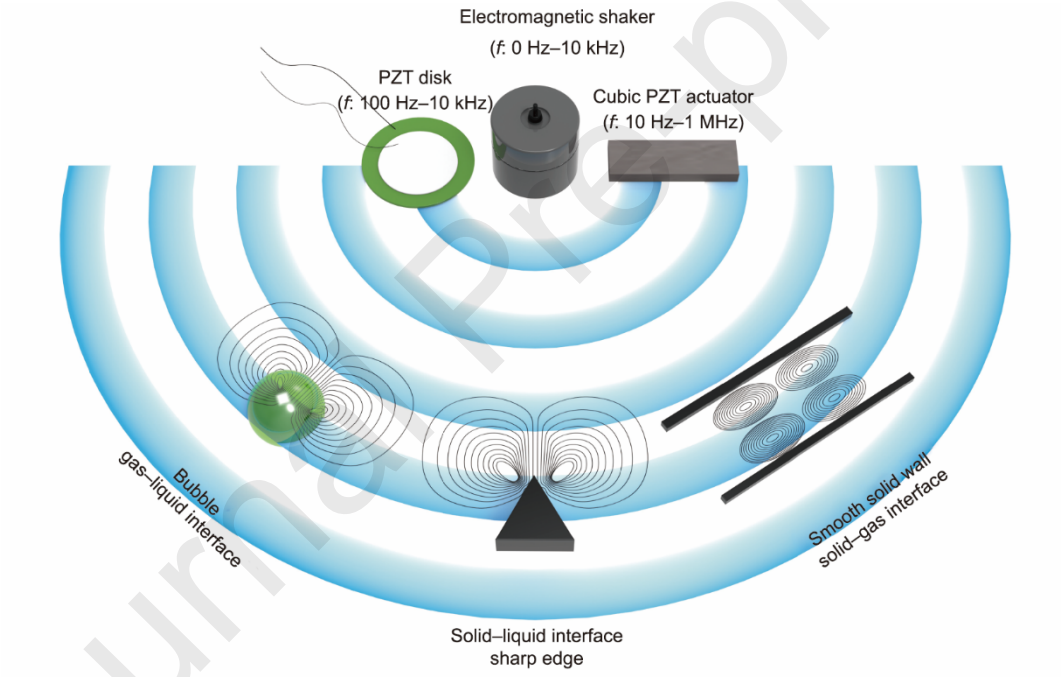

Fig. 3. Common vibration actuators available for generating audible frequencies.

A common method for integrating PZT actuators within devices is to bind them at a specific location on the substrate, which constitutes one of the walls containing the liquid. As shown in Fig. 4(a), a commercial PZT thin-disc-shaped transducer may be glued directly onto the substrate (glass, in this example). Binding can be either reversible (when common acoustic coupling gels are used) or irreversible (when epoxy or any equivalent glue with a curing agent (hardener) is used). As a counterpart to its irreversibility, the latter case has the advantage of providing a relatively robust mode of energy transfer, as the vibration wave is distributed throughout the substrate wall to reach the fluid–solid boundary. In some studies, the vibration of a part of the wall was observed [46], whereas in others, the resonant vibration of the fluid itself inside the channel was observed [14]. However, to the best of our knowledge, the "optimal" position of the transducer must be determined by trial and error in many situations, although direct vibration measurements have been conducted

by Chindam et al. [65] and Bachman et al. [66]. Vibration measurements may be achieved either by measuring the amplitude of the vibration on the wall using a heterodyne interferometry vibrometer or by direct measurement of the periodic flow. In the latter method, fluid seeded with small particles is visualized using high-speed and high-magnification cameras and lenses. The correspondence between the voltage and vibration amplitude must be precalibrated for each resonance frequency whose use is anticipated in the experiments. Consequently, additional studies are required to enable more robust design and reliable methods for transferring vibrations from solids to liquids.

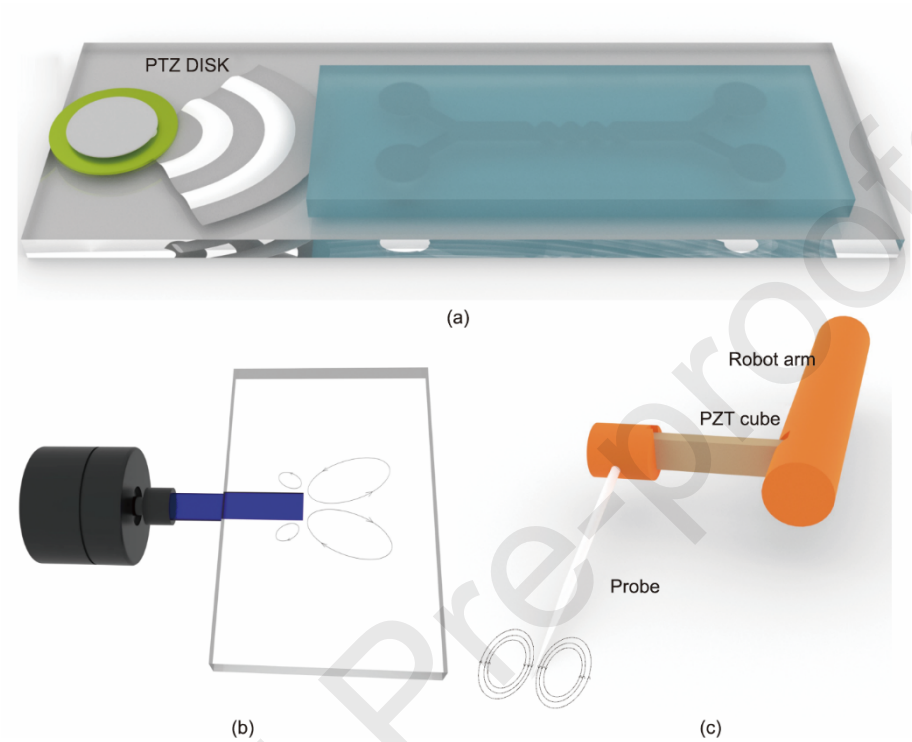

Fig. 4. Several common acoustofluidic devices with low-frequency forcing. (a) Piezoelectric disk attached to a glass slide forming a wall of a microchannel, (b) electromagnetic shaker transmitting the vibration to the fluid via a beam, rod or shaft. Reproduced from Ref. [34] with permission. (c) PZT materials directly integrated with a robot arm to induce streaming near the end of the probe. Reproduced from Ref. [67] with permission.

Electromechanical shakers have been used to induce vibrations at frequencies ranging from a few hertz to several kilohertz. Simple transmission structures, such as cylinders, beams, or shafts, have been attached to shakers to transmit vibrations to the liquid via the no-slip boundary condition [10,34,45], as shown in Fig. 4(b). This configuration benefits from the continuous and accurate control of the amplitude and frequency of vibrations over a wide range, exempt from the constraint of discrete resonant states, although the configuration generally fails to sustain vibrations above 20 kHz. In addition, as shown in Fig. 4(c) [67], in recent studies using robot arm-assisted tip manipulation [67,68], PZT cubes or discs were positioned close to and directly on the arm to excite vibration at the probe. This simple method is efficient and robust for prescribing localized streaming flows.

Table 2. Classical excitement parameters of acoustic streaming.

Vibration source	Frequency	Type of coupling	Main application	Type of interface
Buzzer	2.5 kHz	Attachment on substrate	Mixing miscible fluids [14]	Solid–Liquid

	3.2 kHz	Attachment on substrate	Accomplishing real-time characterization of 4-methylumbelliferyl-β-D-glucuronide [56]	Solid–Liquid
	1–5 kHz	Attachment on bottom of channel	Bubble generation [57,58]	Gas–Liquid
	4.3 kHz	Attachment on side of channel	Fabricating zinc oxide nanoarrays [59]	Solid–Liquid
	4.0 kHz	Attachment on side of channel	Fabricating nanoparticles [60]	Solid–Liquid
	2–5 kHz	Attachment above channel	Accelerating mixing of bacterial cells (Escherichia coli K12) matrix suspended in blood [61]	Gas–Liquid
	1 kHz	Attachment above channel	Pre-treatment before optical detection [62]	Gas–Liquid
	280 Hz	Beams	Enhancement of heat transfer [63]	Solid–Liquid
Mechanical motion from vibrator	60 Hz	Periodic movement from the bottom of container	Tape-cast anode supports [64]	Solid–Liquid
	5–60 Hz	Oscillating cylinder immersed within fluid	Demonstrating the inner acoustic boundary [10]	Solid–Liquid
	15–120 Hz	Vibrating beam in a Hele–Shaw cell	Generating vortices in a Hele–Shaw cell[34]	Solid–Liquid

2.2.2. Location where streaming appears: interfaces and boundaries

Acoustic streaming is usually classified as either the Rayleigh (or Rayleigh–Schlichting) or Eckart type, depending on the location where most of the acoustic energy is dissipated. Below the ultrasonic range, and for most typical fluids, dissipation generally occurs in the vicinity of boundaries, thus generating Rayleigh streaming. In wall-bounded flows, the boundaries naturally impose a no-slip condition, thereby generating sharp velocity gradients perpendicular to the walls. In the case of vibrating immersed bubbles [69–71], the free surface acts as a membrane that

periodically and successively extrudes the fluid, pulling it in a direction normal to the surface. This periodic motion also generates a VBL around the bubble, where the acoustic energy is dissipated and transformed into fluid motion.

However, observations have indicated that the generation of a VBL around a solid boundary or interface is not a sufficient condition for the existence of streaming. In the classical experiment of an immersed cylinder vibrating in a direction perpendicular to its axis [10,26–29], or that of a vibrating immersed sphere [31,32], streaming is manifested as pairs of counter-rotating vortices around the object. Conversely, in the case of an immersed vibrating beam [34] or probe [67], streaming is only generated at the end of the beam and not along its main length. When a sphere is replaced by an elliptical spheroid, the streaming vortices drift toward the major axis of the spheroid [72].

In a Kundt's tube, the pairs of vortices appear with spatial periodicity at intervals of $\frac{\lambda}{2}$, but if λ is larger than the tube length L, no streaming can be observed. Therefore, in microfluidic channels, given that the speed of sound in water is $c_s \simeq$ 1500 m·s^{-1} under normal conditions, the actuation frequency has generally been taken to be of the order of a few megahertz (for instance, in Refs. [73,74]), so that a matching condition is achieved between the length or width of the channel and $\frac{\lambda}{2}$.

2.3. Dependence of streaming flow on the local geometry

For a clearer understanding of the process and a more accurate prediction of the location where vibrations will be transformed into a stationary directional flow, we refer to Lighthill's approach [6], namely that streaming originates from the Reynolds stress (corresponding to the nonlinear term $(v \cdot \nabla)v$. in the Navier–Stokes (N–S) equations). To generate streaming, the time-average of this term must contain nonzero components. The components of this term may be written as $v_i \frac{\partial v_j}{\partial x_i}$ where i and j cycle through the spatial Cartesian coordinates x, y, or z. This means that to generate streaming, the velocity must vary along each direction in which it has a nonzero component. The walls have the dual function of generating velocity gradients along the normal direction, because of the no-slip boundary condition, and directing the forcing in a direction parallel to the walls. Given these two features, it is clear that any forcing of a homogeneous amplitude along the parallel walls should not generate any streaming. In Kundt's tubes, the observed streaming results from the fact that $\lambda < L$, such that the amplitude of the acoustic forcing varies along the longitudinal direction. However, in most situations of forcing at audible frequencies that involve liquids such as water, $\lambda >> L$. No forcing can arise in such a situation, unless the wall geometry departs from a smooth, straight shape. For example, vibrating immersed objects such as cylinders or spheres can generate streaming because of their nonzero curvature. In the case of channels, streaming can be generated owing to the presence of wall textures because any of these elements is likely to deviate the forcing from a straight direction.

Correspondingly, a few recent studies considered microfluidic channels with one or several sharp edges to generate streaming at $\lambda >> L$ [45,46,75]. The adjective "sharp" here denotes that the element of texture at the wall possesses a radius of curvature $r_c < \delta$. Under this condition, the acoustic (forcing) velocity experiences a strong change of direction near the tip, and the term $(v \cdot \nabla)v$ becomes important in the tip vicinity (as it is associated with an advective centrifugal acceleration [45]), whereas in the absence of any texture (corresponding to a straight wall), the acoustic forcing at long wavelength (equivalent to a low frequency) remains homogeneous and directed toward the wall, generating no streaming. Using experiments and finite element simulations, Zhang et al. [14,76,77] demonstrated that both the orientation of the oscillations and their amplitudes were influenced by the sharp structure, which led to a strong localized deflection of the fluid. The impact of this effect on the streaming depends on the properties of the sharp-edge structure. As shown in Fig. 5, the streaming flow only appears near the sharp edge, whereas it is absent around a smooth round shape under the same acoustic conditions [14]. Two parameters, $2r_c$ (the curvature diameter of the tip of the edge) and α (the angle formed by the tip) are crucial for

the generation of acoustic streaming. As shown in Fig. 5(d), the magnitude of the streaming flow (for the same acoustic forcing) decreases as the ratio $\frac{2r_c}{\delta}$ increases, and especially as it passes a value of 1. This provides a crucial geometrical criterion for exciting a streaming flow at an audible frequency. Various experimental and numerical studies [14,46,75–77] found that the streaming efficiency improves as the angle α decreases. In slightly different geometries, micro-obstacles fabricated within the channel allow the generation of intense local streaming, which can be converted into hydrodynamic tweezers [78].

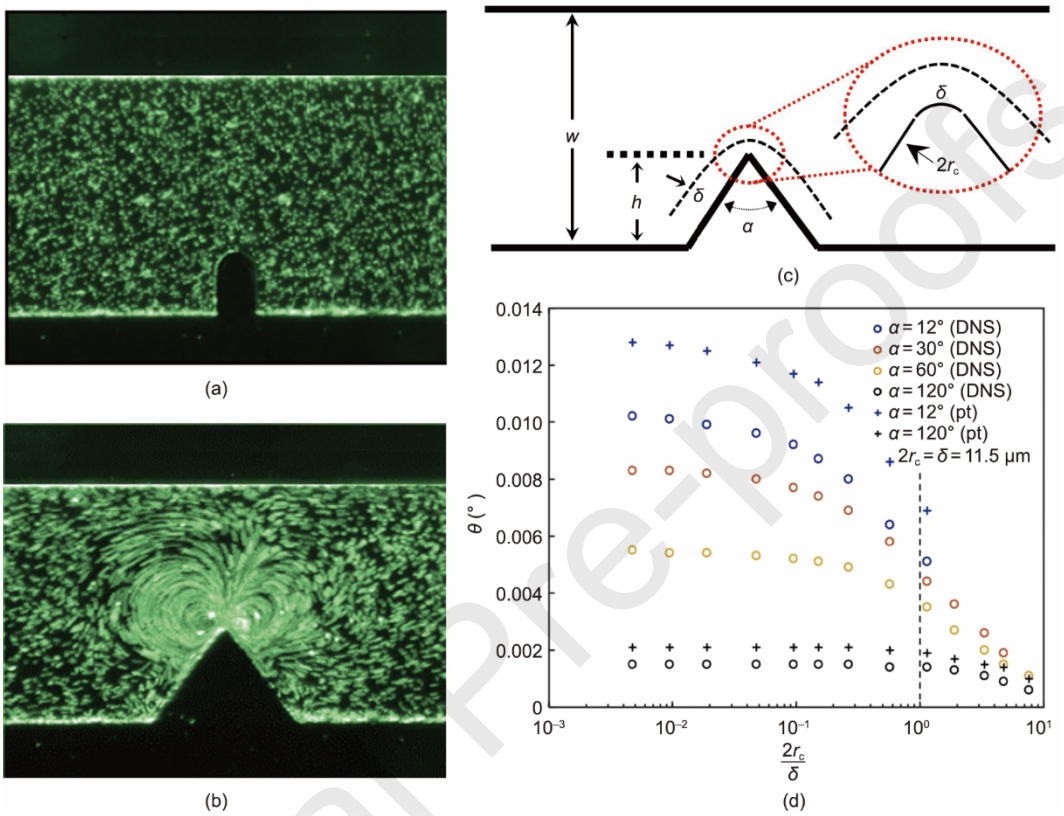

Fig. 5. Mechanism for a sharp obstacle on the wall of a micro-channel inducing streaming in a long wavelength situation ($\lambda \gg L$). (a, b) Streaming flow induced by periodic longitudinal forcing. Reproduced from Ref. [14] with permission. (a) When the obstacle is smooth ($r_c \gg \delta$), no streaming is observed, (b) whereas when the obstacle is sharp ($r_c < \delta$), a streaming jet is projected from the tip, (c) schematic of critical geometrical parameters, (d) coefficient $\theta = \frac{\partial v_s}{\partial v_a^2}$ versus dimensionless curvature diameter at the tip $\frac{2r_c}{\delta}$, quantifying the efficiency of the generation of streaming, for various values of the tip angle α. The plots show a drop of streaming strength as r_c becomes larger than δ. These results were extracted from numerical simulations in Ref. [76].

2.4. Theoretical elements of acoustofluidics at audible frequencies

In this section, we present the fundamental equations governing acoustofluidics in the audible frequency range. From a theoretical perspective, the equations governing acoustic streaming are similar for the audible and ultrasonic ranges [51]; for instance, Rayleigh streaming appears in the description of both situations. In the ultrasonic range, Eckart streaming is observed if the wave-attenuation length is comparable to or smaller than the fluid domain size. This is typically the case for water at frequencies as high as several tens of megahertz, or for more viscous liquids such as glycerin if f is higher than a few hundred kilohertz. For very intense forcing, such that the Mach number (Ma) is of the order of unity, compression effects may become non-negligible; however, this scenario is beyond the scope of our review. Hence, the fluid is generally treated as incompressible in this review, because Ma remains much smaller than unity.

The classical framework describing acoustic streaming decomposes the primary quantities (velocity, pressure, and density) into periodic and stationary time-averaged components. This is a classic example of a perturbation method, in which the streaming velocity is assumed to be substantially smaller than the acoustic (forcing) velocity.

2.4.1. Perturbation theory (PT)

We perform the following decompositions for the velocity (v) and pressure (p) fields:

$$v = v_{\mathrm{a}}e^{-i\omega t} + v_{\mathrm{s}} \quad (2)$$

$$p = p_0 + p_{\mathrm{a}}e^{-i\omega t} + p_{\mathrm{s}} \quad (3)$$

where $v_{\mathrm{a}}e^{-i\omega t}$ and $p_{\mathrm{a}}e^{-i\omega t}$ correspond to the oscillatory, time-periodic fields and v_{s} and p_{s} refer to the stationary fields. The background pressure p_0 is homogeneous and is considered to be equal to the atmospheric pressure, whereas the background velocity v_0 is assumed to be null.

For an incompressible fluid, the Navier–Stokes equations are:

$$\frac{\partial v}{\partial t} + (v \cdot \nabla)v = -\frac{1}{p}\nabla p + \nu\nabla^2 v \quad (4)$$

$$\nabla \cdot v = 0 \quad (5)$$

Substituting Eqs. (2) and (3) into Eq. (4) yields:

$$\frac{\partial v_\omega}{\partial t} + \left\{\left[v_{\mathrm{s}} + \mathrm{Re}(v_{\mathrm{a}}e^{-i\omega t})\right] \cdot \nabla\right\}\left[v_{\mathrm{s}} + \mathrm{Re}(v_{\mathrm{a}}e^{-i\omega t})\right] =$$

$$-\frac{1}{\rho}\nabla\left[p_{\mathrm{s}} + \mathrm{Re}(p_{\mathrm{a}}e^{-i\omega t})\right] + \nu\nabla^2\left[v_{\mathrm{s}} + \mathrm{Re}(v_{\mathrm{a}}e^{-i\omega t})\right] \quad (6)$$

where Re(·) is the real part of the expression, v_{a} represents the forcing velocity.

The equation can be separated into time-dependent and steady parts:

$$i\omega v_{\mathrm{a}} + (v_{\mathrm{s}} \cdot \nabla)v_{\mathrm{a}} + (v_{\mathrm{a}} \cdot \nabla)v_{\mathrm{s}} = -\frac{1}{\rho}\nabla p + \nu\nabla^2 v_{\mathrm{a}} \quad (7)$$

$$(v_{\mathrm{s}} \cdot \nabla)v_{\mathrm{s}} + \frac{1}{2} < \mathrm{Re}[(v_{\mathrm{a}} \cdot \nabla)v_{\mathrm{a}}^*] > = -\frac{1}{\rho}\nabla p_{\mathrm{s}} + \nu\nabla^2 v_{\mathrm{s}} \quad (8)$$

$$\nabla \cdot v_a = 0 \quad (9)$$

$$\nabla \cdot v_s = 0 \quad (10)$$

where Eq. (7) represents the time-periodic part of the momentum conservation equation ($e^{-i\omega t}$ has been neglected for simplicity) and Eq. (8) represents the steady part. The term $\frac{1}{2}(\mathrm{Re}((v_{\mathrm{a}} \cdot \nabla)v_{\mathrm{a}}^*))$ is the time-averaged Reynolds stress force. As explained above, it assumes nonzero values in the vicinity of regions with inhomogeneous velocity gradients.

In the framework of PT ($v_{\mathrm{a}} \gg v_{\mathrm{s}}$), the other advective nonlinear cross-terms $(v_{\mathrm{s}} \cdot \nabla)v_{\mathrm{a}}$ and $(v_{\mathrm{a}} \cdot \nabla)v_{\mathrm{s}}$ are neglected in Eq. (7). For the same reason, $(v_{\mathrm{s}} \cdot \nabla)v_{\mathrm{s}}$ is neglected in Eq. (8).

In this framework, a simple scaling law for the streaming velocity can be deduced from Eq. (8), by requiring that the forcing velocity v_{a} varies along a typical length scale of d and that v_{s}

experiences significant variations on the scale of the VBL(δ), and also by recalling the expression for δ in Eq. (1), yielding:

$$v_s \sim \frac{v_a^2}{\omega d} \quad (11)$$

which suggests a quadratic dependence on the forcing velocity and streaming flow, independent of viscosity. We also note that the streaming velocity scales as the inverse of the forcing frequency at a constant v_a. This scaling is also of interest in acoustofluidics at audible frequencies.

2.4.2. Limit velocity method (LVM)

A classical method for simplifying the solution of the above equations has been proposed in various studies [5,79]. The method is applicable in situations where the thickness of the VBL, δ, is significantly smaller than other relevant length scales. The method is premised on the assumption that the flow is irrotational except in the thin boundary layer (with a thickness of approximately δ) that exists along the surfaces of vibrating objects or solid walls. By eliminating the finer detail of the full flow structure within the VBL, this approach proposes that the resulting time-periodic flow is modeled using the spatial distribution of the slip velocity along the walls. The advantage of this approach is that it allows the use of a potential function, which is a common tool in irrotational flows. In turn, the slip velocity v_1 is generated by the continuity of the time-periodic flow field in the entire fluid domain. The following expression has been proposed for the slip velocity [80]:

$$v_1 = \frac{3}{4} v_a^* \frac{dv_a}{dx} \quad (12)$$

where v_1 is the velocity–slip boundary condition required for the solution of the streaming velocity field in Eqs. (8) and (10) in terms of v_s.

2.4.3. Direct Navier–Stokes (DNS) solution

When the geometry is sufficiently complex or when the streaming velocity cannot be considered small compared to the forcing velocity (v_s and v_a can locally be of comparable magnitude), the perturbative approach is no longer accurate, and the solution of the full N–S equations is required.

In practice, this consists of solving the N–S equations directly using dedicated commercial or open-source solvers or a custom-made code. The acoustic waves can be generated in different ways, either by imposing vibrations on the solid and enabling their energy to leak partially or totally into the fluid, or by prescribing a pressure wave in the fluid associated with a perfectly matched layer (PML) boundary condition at the walls.

In the audible range, it is generally true that $\lambda \gg L$ and $\lambda \gg \omega$, so that the forcing velocity can be applied in a simpler way by prescribing an oscillating velocity as a boundary condition at the ends of the fluid domain. The success of this approach at predicting streaming flow has been supported by several studies [45,76] based on comparisons with experimental results. This technique allows the extraction of the streaming flow alone by computing the time average of *v* over one or several periods, as well as the time-varying component.

Many open-source or commercially available software packages may be used to extract and trace the Lagrangian velocity as well as the Eulerian velocity. This enables a direct comparison with experiments in which the velocity fields are generally deduced from the trajectories of advected particles.

In the context of streaming generated at a large forcing amplitude, such that v_s is (at least locally) no longer small compared to v_a, the solution of the full N–S equations is more reliable than the perturbative method for predicting the flow, for a relatively large range of forcing amplitudes. This is particularly relevant to the audible frequency range. Zhang et al. [76] obtained a solution of

the full N–S equations using finite-element software by computing the streaming flow near a sharp edge for a large range of parameters, demonstrating the limitations of PT and, in particular, the necessity of retaining all the terms in Eqs. (7) and (8).

Furthermore, this method has recently led to previously unreported trends at relatively high forcing amplitudes [55]. First, the quadratic relationship between v_s and v_a (Eq. (11)) still holds, but only within a limited amplitude range. The relationship between v_s and v_a then becomes linear above a threshold amplitude, with a subtle crossover between them. Second, the streaming flow can lose its left–right symmetry under sufficiently strong forcing. Both behaviors can be explained by the fact that v_s locally becomes of the same order as v_a. Hence, if the term $(v_s \cdot \nabla) v_s$, representing the self-advection of the streaming flow, is no longer negligible in Eq. (8) the scaling of Eq. (11) should no longer hold. Furthermore, if the terms $(v_s \cdot \nabla)v_a$ and $(v_a \cdot \nabla)v_s$ are no longer negligible in Eq. (7), the advection of force by the streaming flow becomes substantial. This can lead to a deflection of the forcing direction and a break-up of the initial symmetry of the streaming jet. These facts confirm that computing the full advective terms in the N–S equations is necessary [55].

2.4.4. Maximum streaming velocity

The magnitude of the streaming flow is generally quantified by extracting the maximal value of v_s. The location where this maximal value is found can vary with the geometry considered, but it is generally at a distance approximately equal to δ from the vibrating object or walls [10,14,26]. Using an analytical approach, Orosco and Friend [81] extracted the velocity, pressure, and density partitioning, decomposed the mass and momentum conservation equations, and simplified the equations by assuming that the streaming flow is steady in the semi-infinite domain. A solution for the inviscid situation was obtained as follows:

$$v_{s,\text{invisc}} = v_a \sqrt{\frac{1}{2}[1 - \exp(-2\alpha x)]} \quad (13)$$

where $\alpha = \kappa_i k$ is the absorption coefficient, κ_i the complex wave number, k the acoustic wave number and, v_a the magnitude of acoustic wave velocity. Based on the above expressions, they expressed the maximum velocity

$$v_{\max} = v_a/\sqrt{2} \quad (14)$$

Although the validation of Eq. (13) only covers specific situations constrained by strong assumptions, and the limit expressed by Eq. (14) appears to be independent of the parameters in the constitutive equations, as validated by the experimental results in Ref. [81] (Fig. 6 [14,77,82–87]), where Eq. (13) appears as Eq. (14). The measurements obtained show that the maximal velocity of sharp-edge streaming (observed in [14,77]) in the kilohertz range (2.5 kHz) is very close to the maximum velocity. This suggests that sharp-edge streaming at an audible frequency can approximate an optimal efficiency in generating a streaming flow from an acoustic wave.

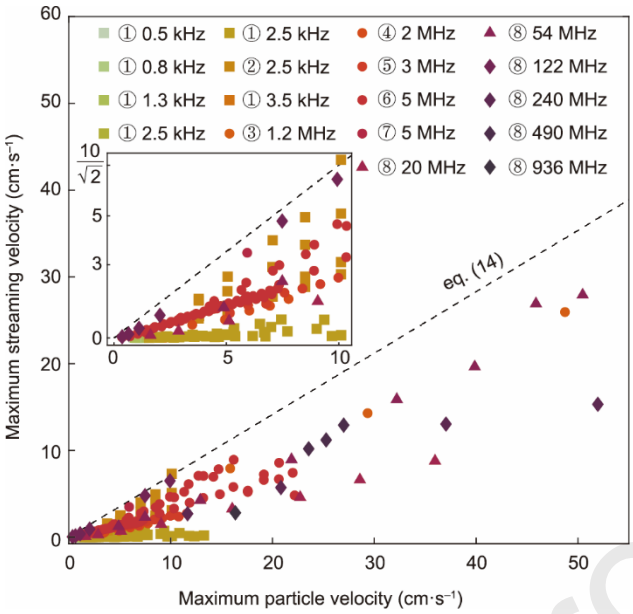

Fig. 6. Various streaming flows (quantified by their maximal velocity) bounded by the theoretical maximum value extracted from the study by Orosco and Friend [81], see Eq. (14). The survey includes 18 data sets spanning eight different studies. Data marker symbols essentially correspond to increments in frequency on a log scale: $(\square)$:$f < 1$ MHz, $(\circ)$:$f \in (1,10)$ MHz, $(\triangle)$:$f \in (10,100)$ MHz, and $(\diamond)$:$f \in (100,1000)$ MHz. The data inserted come from: ① Zhang et al. [77], ② Zhang et al. [14], ③ Makarov et al. [82], ④ Moudjed et al. [83], ⑤ Frenkel et al. [84], ⑥ Mitome [85], ⑦ Kamakura et al. [86], and ⑧ Dentry et al. [87].

2.5. Relevant dimensionless numbers in audible acoustofluidics

In this subsection, we define and examine several dimensionless numbers relevant to acoustofluidics to elucidate the characteristics and advantages of forcing at audible frequencies. As a first step in this qualitative analysis, we list the different length scales, time scales, and velocities involved, grouping them according to their relation to the acoustic wave/mechanical vibration forcing, geometry, or induced flow, respectively.

We may add here the length associated with the wave attenuation, L_{att}:

$$L_{\mathrm{att}} = \frac{2\rho c_s^3}{(2\pi f)^2 \frac{4}{3}\eta + \eta_B} \quad (15)$$

where η_B denotes the bulk viscosity, whereas $\eta = \rho\nu$ is the shear viscosity. In the audible range, even for viscous liquids such as glycerin, L_{att} is generally far greater than any other length scale. It is only as f exceeds several tens of megahertz (for water) or several hundred kilohertz (for glycerin) that wave bulk attenuation becomes significant, with Eckart streaming dominating.

Several dimensionless numbers may be defined based on these quantities. First, various ratios among the length scales can be used to define the typical regime to which a streaming flow is assumed to belong.

For example, when the ratio $\frac{L}{\delta} \gg 1$, one observes Rayleigh–Schlichting streaming, consisting of a rotational flow in the inner VBL (Schlichting vortices) together with an irrotational outer flow (Rayleigh streaming). Conversely, when $\frac{L}{\delta} \simeq 1$, the VBL expands over the entire fluid domain and only Schlichting streaming is observed (see the Ref. [29] for an immersed vibrating cylinder).

The ratio $\frac{d}{\delta}$ is also important. In the literature, this is denoted by the Womersley number (Wo). The Stokes number β, equal to the square of this ratio, is more often encountered in the literature.

This number emerges from the instationary N–S equations (Eq. (7)) as a dimensionless number that expresses the relative importance of instationarity and viscous effects:

$$\beta = \frac{\rho v_a \omega}{\eta v_a / d^2} = \left(\frac{d}{\delta}\right)^2 \quad (16)$$

Classically, several Reynolds numbers used to characterize the flow structure may be defined by considering either the instationary part of the N–S equations (Eq. (7)) or the stationary part (Eq. (8)). The Reynolds number, which is based on the acoustic velocity, compares the relative importance of convection with respect to the diffusion of momentum in the instationary flow field:

$$\mathrm{Re}_1 = \frac{\rho A \omega d}{\eta} = \frac{A \omega d}{\nu} = \frac{v_a d}{\nu} \quad (17)$$

Recalling the expression of δ, this Reynolds number may also be expressed as:

$$\mathrm{Re}_1 = \frac{Ad}{\delta^2}$$

The Reynolds number may also be built on the streaming flow. Stuart [28] proposed the following expression:

$$\mathrm{Re}_s = \frac{v_a^2}{\omega \nu} \quad (18)$$

which, according to the scaling of Eq. (11), may also be expressed as:

$$\mathrm{Re}_s = \frac{\rho v_s d}{\eta} \quad (19)$$

where v_s appears explicitly in the expression.

Wang and Stuart's theoretical studies [27,28] showed that, in the case of immersed vibrating cylinders, the streaming flow regime is governed by both β and Re_s. When $\beta > 1$ and $\mathrm{Re}_s < 1$, the effect of the object curvature is relatively weak and the vorticity is confined within a thin VBL of thickness δ around the object. This condition is generally fulfilled using a Kundt tube or a straight channel. When both $\beta > 1$ and $\mathrm{Re}_s > 1$, a second boundary layer appears outside the inner one, as vorticity is then advected away from the wall. Tatsuno [29] demonstrated the presence of this outer streaming layer experimentally; the size of the layer is predicted to scale approximately as $d(\mathrm{Re}_s)^{-1/2}$. In a subsequent study, Tatsuno and Bearmann [30] conducted a more extensive investigation of different instationary and steady streaming flow regimes over a large range of forcing amplitudes. In particular, they investigated vortex shedding, which can substantially influence the intensity and shape of streaming vortices.

Notwithstanding these results, the condition that $\mathrm{Re}_s > 1$ does not necessarily imply that the condition $v_a \gg v_s$ is no longer satisfied. When the forcing amplitude is strong enough that $v_s \simeq v_a$, the outer vortices tend to stretch in the direction of the vibration [10,34], as a consequence of the importance of the self-advection of the streaming flow. However, Bahrani et al. [10] reported that this stretching becomes significant at $\mathrm{Re}_s > 4$. The condition $v_s \simeq v_a$ is also dependent on the value of β, via the curvature radius of the object (Eq. (11)).

The situation $\beta < 1$ is encountered in microfluidic channels embedded with sharp textures, as mentioned above [14,45,46,55,75–77,88,89]. In this situation, $d \ll h$, and generally $h \gg \delta$. Therefore, the inner VBL appears only along straight walls and does not produce streaming, as explained above. Strong streaming is primarily observed near the tips of the structures. Furthermore, the situation $\beta < 1$ tends to favor vortex shedding (in the instationary flow), so that more complex, even unstable, flows can be generated.

These conditions are favored by acoustofluidics at audible frequencies. For water, δ = 170 μm at 10 Hz and 17 μm at 1 kHz, facilitating the creation of sharp edges using common techniques such as precision machining, 3D printing, or photo-lithography. However, δ decreases to 0.56 μm at 1 MHz; consequently, it becomes almost impossible to satisfy the sharpness condition $\beta < 1$ at such high frequencies using currently available techniques. These limitations also apply to the geometry of microposts embedded within the channel [78].

A further advantage of audible acoustofluidics is that it allows the prescription of relatively large-amplitude waves or vibrations for a given power input. In the majority of forcing devices, power is generally proportional to the square of v_{a}^2. Therefore, decreasing the frequency at constant power increases the value of A. For immersed vibrating objects, an interesting scenario occurs when the amplitude is comparable to the object size. The ratio between the two scales may be quantified in the form of the Keuleghan–Carpenter (KC) number, which also quantifies the ratio between advective inertia and instationary inertia:

$$KC = \frac{2\pi A}{d} = \frac{v_{\mathrm{a}}}{fd} \quad (20)$$

Given the scaling law for v_{s} (Eq. (11)) for a fixed value of v_{a}, the velocity v_{s} increases as f decreases. To date, very few studies have addressed the scenario where $\mathrm{KC} > 2\pi$ in the context of streaming. The majority of studies have been dedicated to the problem of vortex shedding and boundary layer separation in the instationary flow [30]. Very little is known about the averaged flow that arises from more complex instationary flows, such as the asymmetric jets generated in sharp-edge streaming at low frequencies and high amplitudes [55].

For purely kinematic reasons, and given the previous analysis on the importance of the advective term $(v_{\mathrm{s}} \cdot \nabla)v_{\mathrm{s}}$, it may be relevant to define a dimensionless number based on the relative magnitudes of streaming and forcing velocities:

$$\gamma = \frac{v_{\mathrm{s,max}}}{v_{\mathrm{a}}} \quad (21)$$

which quantifies the possibility that the cross-advective terms in Eq. (7) and the self-advective term in Eq. (8) acquire significant influence. For classical Rayleigh streaming, $v_{\mathrm{s,max}}$ can be approximated using Eqs. (11) and (12), depending on the geometry. In sharp-edge streaming, the value of $v_{\mathrm{s,max}}$ may be extracted (inter alia) from the analytical formula given by Eq. (22) in Ovchinnikov et al. [45]. In this latter scenario, the bifurcation to an asymmetric jet and vorticity regime was found when v_{s} was of the same order as v_{a}, emphasizing the relevance of the parameter γ in high-amplitude forcing situations.

3. Applications of low-frequency acoustofluidics

Although the detailed mechanisms of acoustofluidics at audible frequencies are still being unveiled, a broad range of applications in various fields have already been conducted. Classical applications in the biological and life sciences, microscale manipulation, and chemistry, respectively, are discussed in the following subsections.

3.1. Biological detection and manipulation

By virtue of the advantages contained in their miniaturization, small-volume reagent consumption, and low cost, coupled with the point-of-care test (POCT) concept, microfluidic chips have accelerated the development of portable biomedical tests in recent years. As active agents for manipulating fluids and particles inside channels, the vortex-like streaming flows described in the previous sections have been involved in many test processes; for example, in the enhancement of mixing to accelerate the combination of biomarkers and cancer cells [90–92], or the manipulation of bioparticles at the microscale [93–95]. Huang et al. [96] developed an acoustofluidic sputum liquefier that uniformly dilutes sputum samples at a high throughput and considerably lowers their

viscosity. These successful studies have demonstrated the possibility of developing low-frequency streaming flows as versatile tools for biological research and biomedical purposes. In addition, in contrast to acoustofluidics in the ultrasound range, the characteristics of low-frequency acoustofluidics include stability, bio-friendliness, and avoidance of the side effects encountered at higher frequencies, such as shock waves from cavitation and local heat from wave dissipation.

3.1.1. Detection of biomarkers

As shown in Fig. 7(a), Chen et al. [90] designed a microchamber surrounded by different bubble-liquid interfaces on the walls, seeding the structure with magnetic beads to capture cancer biomarkers. Under a piezoelectric disc working at 5–11 kHz, bubbles of different sizes were activated at their respective Minnaert resonance frequencies and the detection of the biomarkers was completed within minutes [90,91]. The results of these studies indicate the great potential of multiple biomarkers in POCT diagnostics. Surendran et al. [62] attempted to conceptualize other types of biodetection. As shown in Fig. 7(b), they presented a real-time biosensor based on the principle of colorimetric optical absorption by virtue of acoustofluidic-enhanced mixing, which enabled a uniform concentration to be established within the fluid. Their device achieved the rapid detection of potassium in whole saliva samples. Specifically, a liquid test sample (Fluid 1) and its corresponding chromogenic agent (Fluid 2) were mixed using acoustic waves generated by a piezotransducer at 1 kHz. Similarly, fluidic mixing experiments were conducted with sheep blood samples in a microchamber (Fig. 7(c)), demonstrating that acoustic mixing not only enhanced the efficiency of bacterial cell capture, but also provided a low shear strain field where bioparticles usually remained intact (unharmed) after the mixing process [61]. Gao et al. [97] mounted a 96-well plate between loudspeakers to generate acoustic streaming using a standard enzyme-linked immunosorbent assay (ELISA). They found that streaming generated by vibrations from 125–150 Hz increased the initial rate of antibody-antigen binding by more than 80% and total binding by more than 50%, indicating that acoustic streaming can increase the sensitivity of ELISA and shorten the binding time from 45–60 min to approximately 15 min.

In addition to biomarkers, bioreactions that utilize micromixing at audible frequencies have been reported in an increasing number of studies. Liu et al. [98,99] fabricated a highly integrated platform for DNA analysis consisting of sample preparation, Polymerase Chain Reaction (PCR), and DNA array detection. On this biochip, a buzzer was attached to a local area of interest to excite microstreaming and enhance the capture of target cells from whole blood samples. Overall, that strategy shortened the time required for DNA hybridization. Kardous et al. [100] attached a piezotransducer to the bottom of a commercial gold surface plasmon resonance imaging (SPRi) chip to produce a chaotic flow in every spotted droplet. That strategy disrupted the steady state of the Ab grafting reaction and increased the biorecognition performance. Wang et al. [101] designed a type of microfluidic chip for cell lysis assisted by the shear strain from acoustic sharp-edge streaming. They asserted that the lysis efficiency could reach more than 90% and that the platform performed well for adherent and non-adherent cells. Following the same idea, Zhao et al. [102] used a streaming-assisted chip to homogeneously mix stool samples with phosphate buffered saline (PBS) to achieve liquefaction, which may provide a basis for further POCT for stool analysis.

The main purpose of introducing streaming during biological detection is to improve the transfer efficiency from biomarkers to local detectors by a significant amount and to produce a substantial signal at high speed.

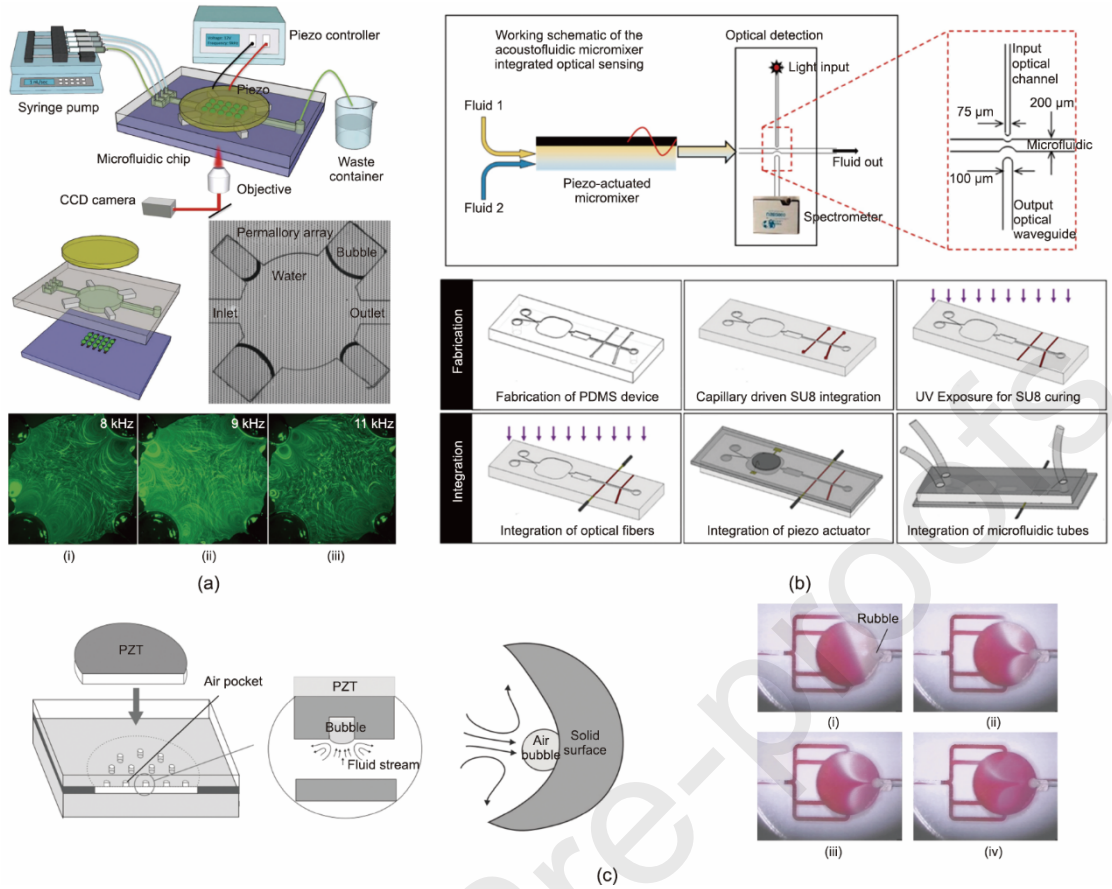

Fig. 7: Enhanced reactions completed within shorter duration by strong mixing generated at audible frequency. (a) A platform integrating magnetic beads to capture multiple biomarkers and micromixing to accelerate this process. Reproduced Ref. [90] with permission. (b) A detection device allowing for detection of potassium by combing a mixing chamber with a fiber probe inserted into the channel. Reproduced Ref. [62] with permission. (c) Strong convection flow induced around a bubble with 1 kHz excitation by attaching a piezoelectric disk to the microchamber. Reproduced Ref. [61] with permission.

3.1.2. Manipulation of biological particles

The generation of vortices by streaming appears to constitute an optimal flow condition, where bioparticles of comparable size whirl around a bounded region of space and cannot readily escape from this region. This makes it possible that, to some degree, trapped targets can move with the interfaces (such as the solid–liquid or gas–liquid (bubble) pattern mentioned above) where streaming is excited, and that the manipulation of a single particle, such as a cell or a small volume of sample, may potentially be achieved in such a scenario. Compared with other state-of-the-art techniques, such as light tweezers, this type of acoustic operation is accomplished by low-magnitude drag forces imposed on the suspensions by the surrounding fluids. This ensures an almost damage-free effect on the targets and low-cost setup requirements in complex processes [103]. These advantages of the trapping and release processes promote the application of streaming in various manipulations.

Marmottant et al. [58, 69] investigated the transport process in a streaming flow around a bubble in microfluidics, targeting bioengineering applications. They trapped a single bubble at the bottom of a microfluidic chamber and observed vesicle formation and lysis. Their work revealed the intriguing possibilities of acoustic control of biological particles. However, the vibrating bubbles were excited at an ultrasound frequency, and the possible cavitation involved could complicate the situation (to some extent) and damage the cells. Considering that the resonance Minnaert frequency f_{M} for a single bubble of radius r_{b} in water under standard conditions is $\frac{3.26}{r_{\mathrm{b}}}$, the same

phenomenon may be realized in a simpler cavitation-free situation at an audible frequency, for millimeter-sized or slightly submillimeter-sized bubbles.

Läubli et al. [104,105] fabricated a channel with bubbles trapped inside an array of grooves on one side and a buzzer attached to the same substrate. Acoustic vibrations induced streaming vortices that trapped plant cells, causing them to whirl. Such manipulation of single cells facilitates 3D fluorescence microscopy to the extent that high-resolution 3D optical reconstructions of nontransparent samples may be demonstrated. Chung and Cho [106] combined electrowetting-on-dielectric (EWOD) electrode bubble transportation with streaming generated around a bubble excited by low-frequency vibrations. They captured, carried, and released particles from a chip. The EWOD patterns were then removed, and a tube filled with gas was introduced. The trapped particles moved with the tube to complete 3D manipulation [107].

Liu et al. [67] first focused on the streaming vortex flow around microbubbles inside a micropipette to control the swirl of objects. As shown in Fig. 8(a), they designed a platform to achieve contactless trapping, transportation, and rotation at the microscale, a core part of which consisted of a micropipette vibrating at 250–375 Hz. The vortex around the micropipette comprised a low-pressure area at the center and surrounding velocity field gradients, which enabled trapping of the targeted particles and their transport through the micropipette [67,108]. In addition to bubble-assisted manipulation, various local solid wall structures have been designed to achieve similar functions.

Lutz et al. [109] developed a method for trapping and resuspending a single cell by streaming flows around pillars immersed in a fluid. They found that the trapping location depended on the oscillation frequency. Furthermore, the trapping force could attain a strength of 30 pN, comparable to that of typical optical tweezers or dielectrophoretic traps. To achieve the parallel multifunctional manipulation of cells (Fig. 8(b)), Xue et al. [110] fabricated polydimethylsiloxane (PDMS) microchannels with a microcavity array and a PZT to induce local microstreaming around the cavities. Using this type of chip, circulating tumor cells (CTC) were trapped and separated with an efficiency of up to 90%. Hayakawa et al. [111] used micropillar patterns with low-frequency vibrations to manipulate oocytes and induce 3D rotations. As shown in Fig. 8(c), they designed a triangular network of pillars, and the trapped cells could move in both the focal and vertical planes of the microscope. In addition, they extended the triangle-like structure to a spiral pattern, and targeted cells were transported toward a single-cell catcher placed at the center of the spiral [112,113].

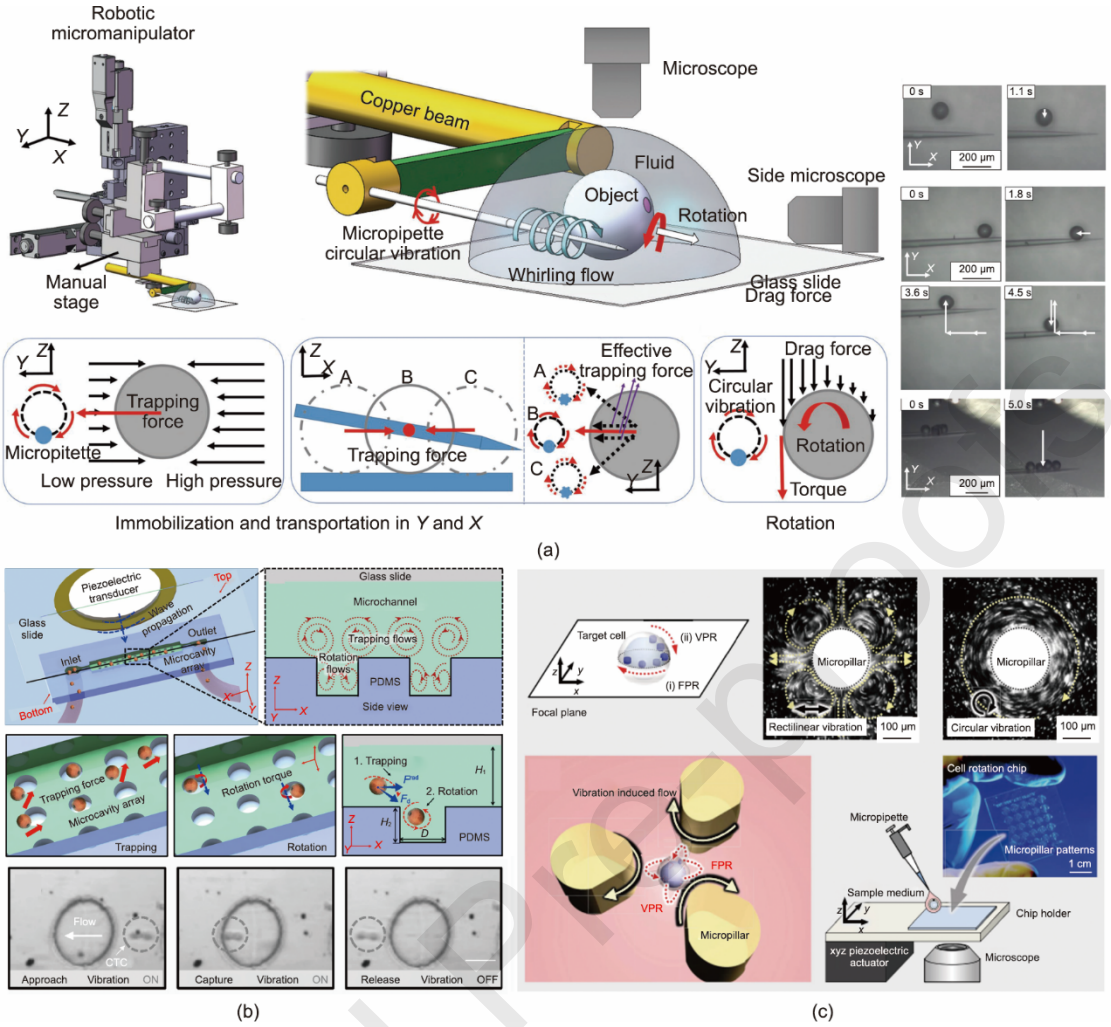

Fig. 8. Manipulation of cells by adjusting the local structures. (a) Platform developed by Liu et al. [67], on which microscale immobilization, rotation, and transport can be achieved with the help of streaming vortices near the tip, F^{rad}: Acoustic Radiation Force, F^{d} : Fluid drag force. Reproduced from Ref. [67] with permission. (b) microchip enabling parallel multifunction based on acoustic microstreaming, consisting of trapping, patterning, separating, and rotating microtargets. Reproduced from Ref. [110] with permission (c) microchip designed by Hayakawa et al. [111] with micropillar patterns to trap and rotate biological cells at the center by streaming flow, FPR(focal plane rotation), VPR(vertical plane rotation). Reproduced from Ref. [111] with permission.

Recently, Ahmed's group [68] developed a liquid manipulation system by integrating robot arms with manipulating needles in which a streaming vortex near the vibrating tip could trap microscale objects. They also applied this system to the mixing of complex viscous liquids. In addition, they designed a chip in which a buzzer was attached to the substrate, enabling the 3D rotational manipulation of various plant species. This platform facilitates fluorescence microscopy and optical reconstruction of samples [104].

3.1.3. Formation of tumor spheroids

Tumor spheroid formation using microfluidic chips has attracted much attention [114,115]. Based on the trapping effect of the streaming vortex, researchers have demonstrated that this type of chip is suitable for cell culture and manipulation. Ozcelik et al. [116] demonstrated the rotation and trapping of model tumor cells (HeLa cells) and the model nematode organism *C. elegans* in streaming vortices generated using 5 kHz acoustic waves in a microchannel with an array of sharp edges. Similarly, as shown in Fig. 9(a) [117], Rasouli et al. designed a simple microchannel structure with multiple gas-liquid interfaces on the side wall, where an induced streaming vortex at 16.1 kHz was used to form the spheroid (Fig. 9(a)). First, dispersed tumor cells were gathered and attracted to the vortex area. Rotation was continued in order to induce intercellular connections. Robust cell

clusters were gradually generated through the incorporation of a bioadhesive such as collagen. The versatility of the platform was demonstrated by its ability to produce MDA-MB-231 and MCF-7 spheroids, multicellular spheroids, and composite spheroids composed of cells and microparticles. Gao et al. [118] designed a microfluidic platform to continuously trap, rotate, and grow cancer cells near a liquid-bubble interface (Fig. 9). They achieved satisfactory integration of the different parts and demonstrated high cell viability using this device.

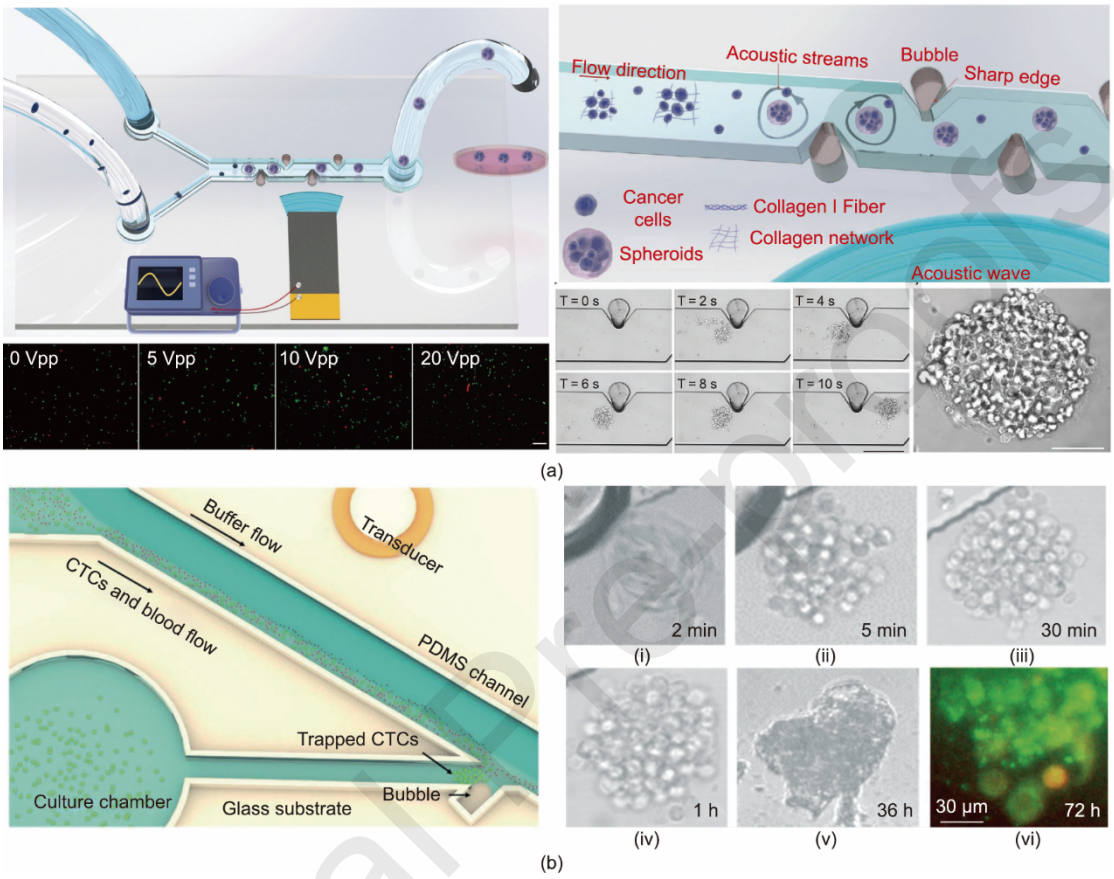

Fig. 9. Trapping and rotation of tumor spheroids achieved by streaming vortices generated at audible frequencies. (a) Microchannel with multiple gas–liquid interfaces on sidewalls to induce microstreaming that simultaneously aggregates cells and generates robust cell clusters. Reproduced from Ref. [117] with permission. (b) Microfluidic chip including a separate trapping part using a gas–liquid interface-induced streaming vortex and an independent culture chamber after aggregation. (b-i) CTCs trapped by acoustic bubbles, (b-ii) CTCs aggregates after 5min, (b-iii, b-iv) formation process of spheroid, (b-v) smooth surface of the spheroid after 36hr, (b-vi) cell-staining images after 72 h of spheroid culture. Reproduced from Ref. [118] with permission.

3.2. Chemical mixing and reaction

The aforementioned limitations, resulting from poor transfer and a slow rate of biodetection by microfluidic chips owing to the low-Reynolds-number flows involved, are challenges that are also faced in chemical reactors at the microscale. Notwithstanding these limitations, the obvious advantages of requiring smaller amounts of reagents and allowing better control of the chemical reactions in microfluidics have motivated an increasing number of studies in this field. To counterbalance poor transfer, an effective solution is to disturb the surrounding fluids through a streaming flow.

Concerning larger-scale reactors, it was shown in experimental studies by Stuart [28], Tatsuno [29], and Tatsuno and Bearmann [30] that the size of the outer vortices could be comparable to the size of the fluid container, and hence, that of a reactor. Bahrani et al. [10] showed that, as the vibrations increased in amplitude, the streaming vortices could be elongated along the axis of

vibration, to a size much larger than that of the vibrating object. These examples suggest that process intensification may be achieved at the (macro)-scale of a reactor.

Solid–liquid and gas–liquid interfaces have both been built inside the channels to induce streaming flows. Ahmed et al. [70] introduced a horseshoe structure at the position where a bubble was trapped and different miscible fluids merged. At a resonance frequency of 100 Hz, mixing was efficiently achieved by streaming near the gas-liquid interface. Ahmed et al.[71] also designed a Y-type channel with grooves on the sidewalls to trap bubbles and excite the streaming flow. Fast and homogeneous mixing of two side-by-side flowing fluids was achieved. Wang et al. [119] designed a chip attached to a buzzer at the bottom wall, vibrating at between 1.5 and 2 kHz; their results revealed satisfactory mixing in various DI water-glycerol solutions, up to a maximum viscosity of 44.75 mPa s.

As discussed previously, owing to perturbations in flows that are caused by streaming, microchannels with sharp-edged arrays have a marked ability to accelerate mixing between miscible fluids. In 2013, Huang et al. [46] were the first to generate a streaming flow near a sharp-edged structure in a microchannel using transducers operating at a few kilohertz. They applied their device to achieve mass transfer. Nama et al. [75,120] built a model to describe the complex mechanisms of mixing and the effects of various parameters and geometrical patterns on the overall performance of acoustofluidic devices. Zhang et al. [89] studied the importance of the spacing between tips in achieving optimal mixing performance. One of the most important aspects of their study (Fig. 10(a)) was the assessment of the mixing through the evaluation of the micromixing time, as introduced by the Villermaux–Dushman method, such that a direct comparison could be made among various micromixers. The obvious advantages of mixing efficiency and economic energy consumption have been demonstrated using micromixers with low-frequency acoustic activation [14].

The attributes of the strong mixing platform described above facilitate its use in the synthesis of materials. Huang et al. synthesized versatile nanoparticles and nanomaterials such as polymeric nanoparticles (Fig. 10(b)), chitosan nanoparticles, organic–inorganic hybrid nanomaterials, metal–organic framework biocomposites, and lipid-DNA complexes [60]. Adjustment of the strength of the streaming flow, the flow rate, composition, and concentration provide this type of platform with a large degree of flexibility for mediating various chemical reactions. Hao et al. [59,121] fabricated a 3D ZnO nanoarray and a 3D plasmonic ZnO–Ag nanoarray based on a similar sharp-edge acoustic streaming-assisted platform. Furthermore, the normal triangle-like edge was replaced with a flower-like pattern to achieve better performance [122]. This type of micromixer was applied to control the synthesis of a 3D ZnO nanorod array, where the mixing of zinc acetate and sodium hydroxide was considerably enhanced by the steaming flow. The three aforementioned studies demonstrated that this type of micromixer has considerable potential for the synthesis of micromaterials and nanomaterials. The same authors reviewed acoustic-assisted microreactors operating at audible and ultrasonic frequencies [123].

Other researchers have conducted interesting studies, as shown in Fig.11 [96, 124–126]. Tang et al. [124], as shown in Fig.11(a), applied a low-frequency acoustic field to control the dispersion of EGaIn metal liquid. The size distributions of metal droplets at different acoustic powers and under different electrochemical conditions were investigated. Furthermore, the chip was used for heavy metal ion detection using the liquid metal microdroplets that had been produced as the working electrode. Ahmed et al. [125] proposed a platform to provide a chemical gradient in a microenvironment by introducing a streaming flow activated by a horseshoe-shaped bubble in the center of a channel. This method may be used to study the intracellular chemotactic behavior. Xie et al. [126] fabricated a channel with sidewalls in which air bubbles were pinned to excite streaming vortices in response to acoustic excitation, as shown in Fig.11(c). This method significantly accelerated chemical extraction in the main channel. Their experimental results showed that the extraction efficiency was dependent on the oscillations of the liquid-liquid interface, which were dictated by the characteristic parameters of the bubble, particularly its volume. Similarly, Huang et al. [96] replaced horseshoe bubbles with sharp edges and designed an array to simulate environments with steep chemical gradients (Fig. 11). Fung et al. [127] attempted to combine jet streaming from an edge structure with membrane filtration. Their experiments showed that jet flow

can efficiently remove layer cake aggregates formed on a microfluidic membrane-on-chip device, with the process occurring in less than 100 ms.

3.3. Micropumping and propelling

When the streaming flow is generated by asymmetric objects, the resulting flow can also be asymmetric, enabling applications in pumping flows or in propelling objects.

Inspired by the phenomenon of jet streaming near orifices mentioned in the previous sections [36–38], Dijkink et al. [128] immersed a tube that was closed at one end and partially filled with gas at the immersed end. When a sound field was added to the liquid that the tube was immersed in, the net momentum from the second streaming flow exerted a force on the tube interface. Feng et al. [129] fabricated suspended microchannels in which bubbles were trapped at the ends. Microstreaming around the bubble interface propelled a microscale robot under external acoustic excitation at 10 kHz or higher. They demonstrated that a strong propulsion force could be achieved by applying a forcing at the natural bubble resonance. This type of artificial swimmer also enables payload carrying. Similarly, Ryu et al. [130] actuated the vibration of bubbles using AC electrowetting, in which the bubbles were trapped on the tip of a metal rod covered with dielectric layers. At 800 Hz, the streaming flow induced around the bubble propelled the metal rod. This type of device was scaled to centimeter size. They also replaced the alternating current AC (AC) electrowetting actuator with a simpler PZT transducer attached to the back of the substrate, which excited the aforementioned bubble. The oscillation modes of the bubble interface were reported in their study. For micron-sized bubbles, the pumping velocity reached 5 $mm \cdot s^{-1}$ under a pressure load of 250 Pa [131].

To the best of our knowledge, Tovar et al. [132] were the first to attempt acoustically assisted pumping in a microchannel. They presented a channel with an array of angled lateral cavities with trapped air bubbles along the flow direction. In their experiments, the platform could drive the fluid at pressures of 350 Pa (Fig. 12(a) [133]). Recently, with the development of sharp-edge acoustic streaming (12(B)), a closed microchannel with asymmetric edges on the wall was designed by Huang et al. [88]. In their study, stable continuous flow rates as high as 8 $\mu L \cdot min^{-1}$ could be generated. Furthermore, the flow rate could be modulated within a wide range, from nanoliters to microliters per second.

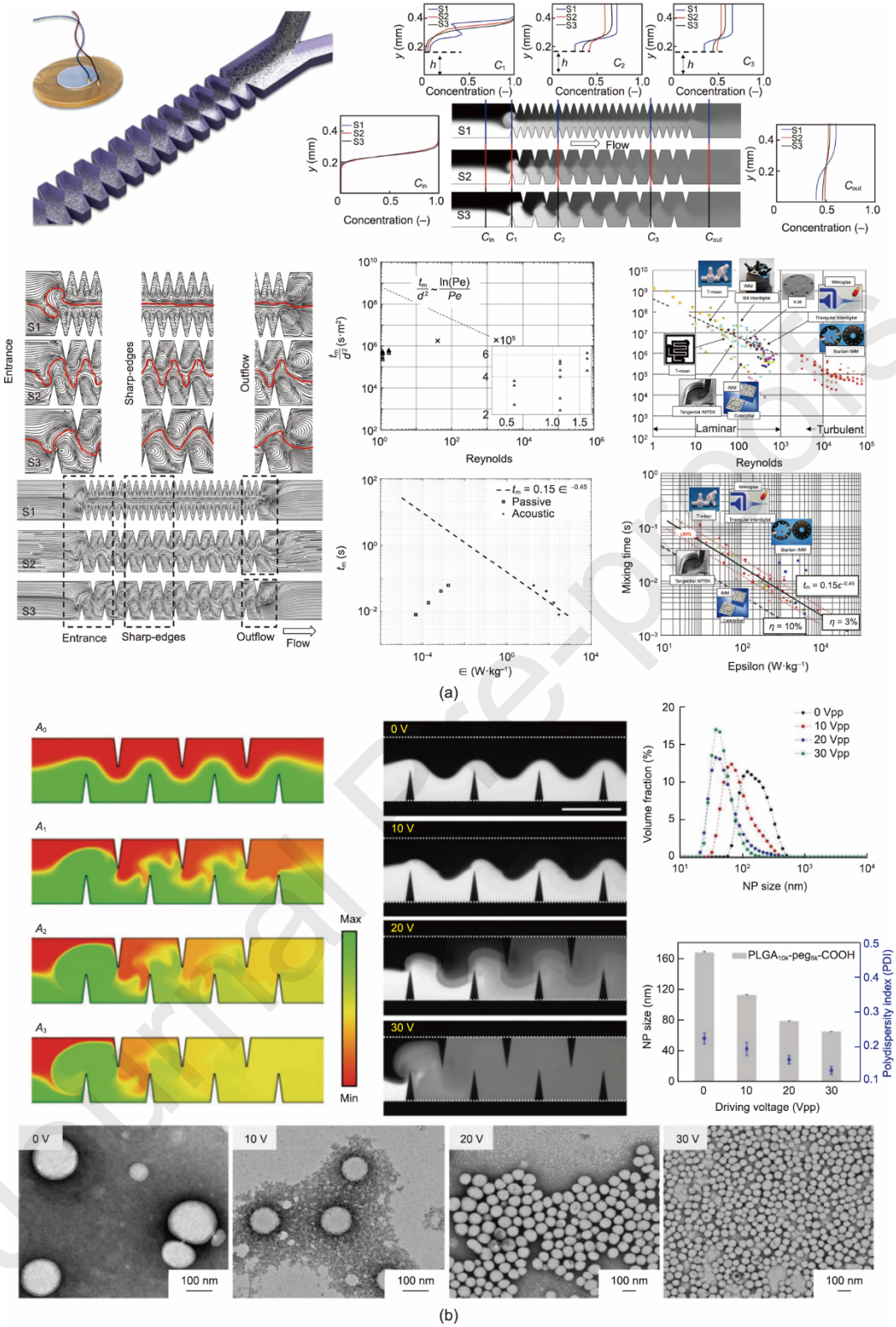

Fig. 10. (a) Rapid mixing by a microchannel with sharp edges and an assessment of the micromixing time allowing for direct comparison with traditional passive micromixers. Reproduced from Ref. [60] with permission. (b) fabrication of nanoparticles with the help of rapid mixing by sharp-edge acoustic streaming. Reproduced from Ref. [89] with permission.

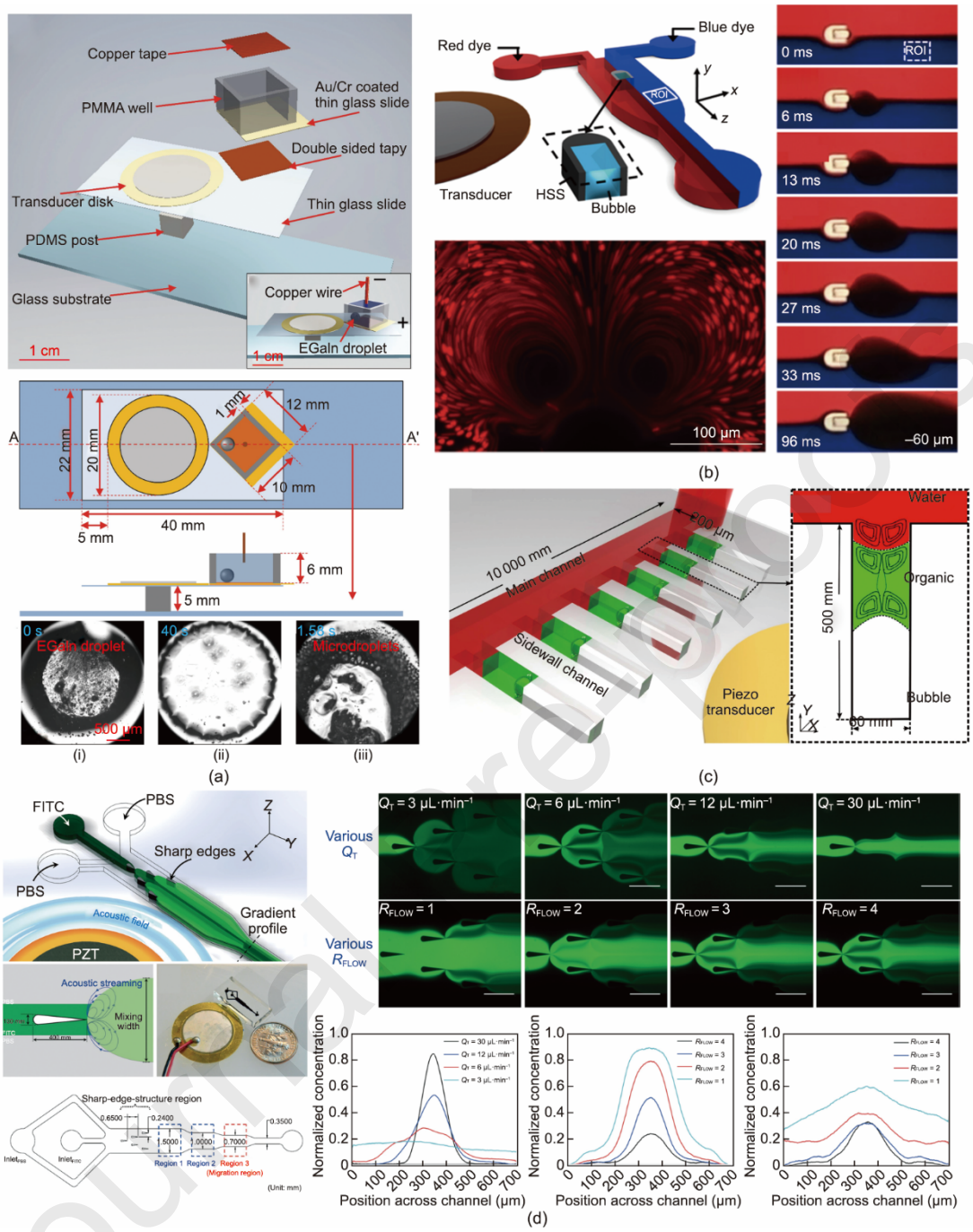

Fig. 11: Audible frequency vibrations producing streaming flow, which enhance chemical reactions. (a) On-chip liquid metal microdroplet production by streaming, Reproduced from Ref. [124] with premission; (b) microchannel with horseshoe bubble trap to excite streaming and modulate the chemical stimulus in the microenviroment, reproduced from Ref. [125] with premission; (c) microfluidic device with sidewall channel, where streaming vortices generated by the oscillation of bubbles lead to mass transfer enhancement and liquid–liquid extraction, reproduced from Ref. [126] with premission; (d) chemical gradient generator controllable in space and time, by virtue of sharp-edge acoustic streaming reproduced from Ref. [96] with premission.

3.4. Heat transfer and control

As stated earlier, Rayleigh–Schlichting streaming dominates at relatively low frequencies; thus, the proposal to exploit streaming to enhance heat transfer from walls to fluids has emerged naturally. The subject is now mature enough to address challenging issues specific to microfluidics (or, more generally, in low-Reynolds-number flows) where the heat transfer rate is generally low. Classical

analysis of heat transfer performance determines the dimensionless Nusselt number, which quantifies the relative importance of convective transfer with respect to diffusive transfer.

Proceeding from the perspective of understanding the fundamental mechanisms governing these flows, Hamilton et al. [54,134] derived an analytical solution for streaming flows confined by parallel plates and then extended their analysis to a gas fluid, where the effects of temperature on compressibility, viscosity, and heat conduction were included. Mozurkewich et al. [135–137] conducted experiments on convective heat transfer around a cylinder and inside a cylindrical resonance tube. Through analytical, numerical, and experimental approaches, Gopinath et al. [7,138–141] obtained the Nusselt number for a wide range of Prandtl numbers owing to acoustic streaming from classical geometries; specifically, a Kundt's tube, a cylinder, and a sphere.

One of the primary advantages attached to the processing of materials in space is the reduction or even elimination of natural convection associated with gravity. However, there have been some indications (for example, in the Apollo 14 experiments) that spacecraft vibrations may cause appreciable thermal convection [142]. Second-order flow generation in the g-jitter, also called gravity modulation in a microgravity environment, has been investigated because it can induce forced heat convection in spacecraft environments. Farooq and Homsy [143] studied the streaming flow in a square cavity, where a temperature gradient interacted with a constant gravity field modulated by a small harmonic oscillation.

More recently, Hirata et al. [144–146] and Dyko et al. [147] explored streaming flow in various dimensions and cavities under gravity modulation. Lappa [148] simulated particle accumulation in streaming flows under frequency vibrations varying from 10–200 Hz, as shown in Fig. 13 (a).

In g-jitter studies, attempts have generally been made to reduce the convection induced by the streaming flow; however, such disturbances have also been utilized to control and enhance heat transfer in confined geometries. As shown in Fig. 13(b), Wu et al. [63] developed a miniature cooling system for microelectronic devices, such as chips, based on a strong streaming flow excited by vibrating beams. The cooling performance associated with a decrease in temperature from 92 °C to 25.6 °C was measured. An analysis of the heat transfer associated with this cooling showed that the enhancement by acoustic streaming between the heat source and the beam could reach 210%. Lambert et al. [149] attempted to introduce a low-frequency oscillating flow into the tube of a solar heater, as shown in Fig. 13(c). Preliminary estimates indicated a significant enhancement of the heat transfer by oscillatory flows, compared with the forced convection of heat by standard unidirectional flows. Furthermore, they found that the absolute maximum of the thermal diffusivity obtained with a viscoelastic fluid was several orders of magnitude larger than that obtained with a Newtonian fluid.

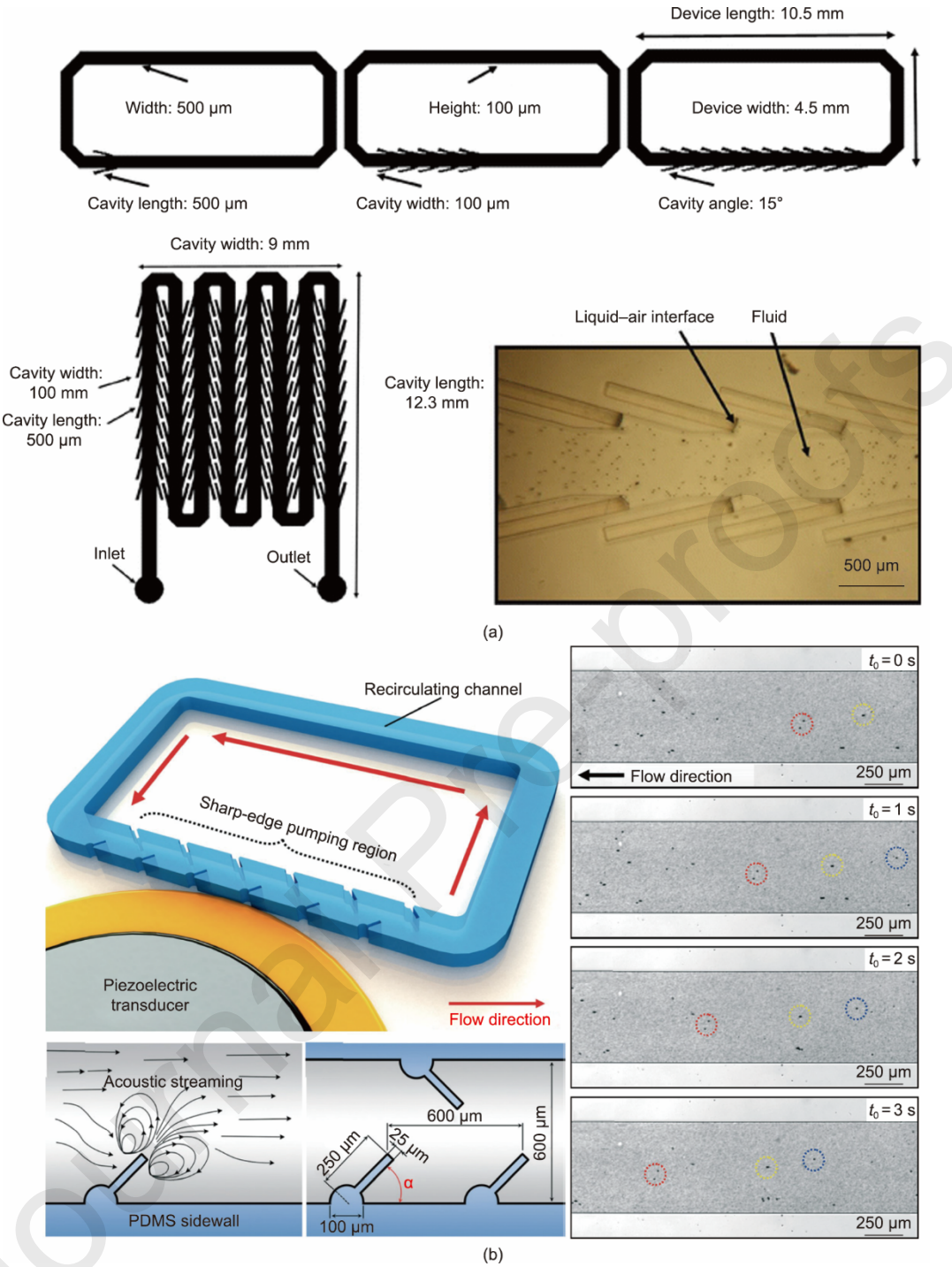

Fig. 12. Valve-free micropumping by acoustofluidics. (a) Microchannel with lateral air cavities to excite microstreaming and to generate a flow rate. Reproduced from Ref. [133] with permission. (b) Closed microchannel with slanted edge structures to induce stable fluid circulation. Reproduced from Ref. [88] with permission.

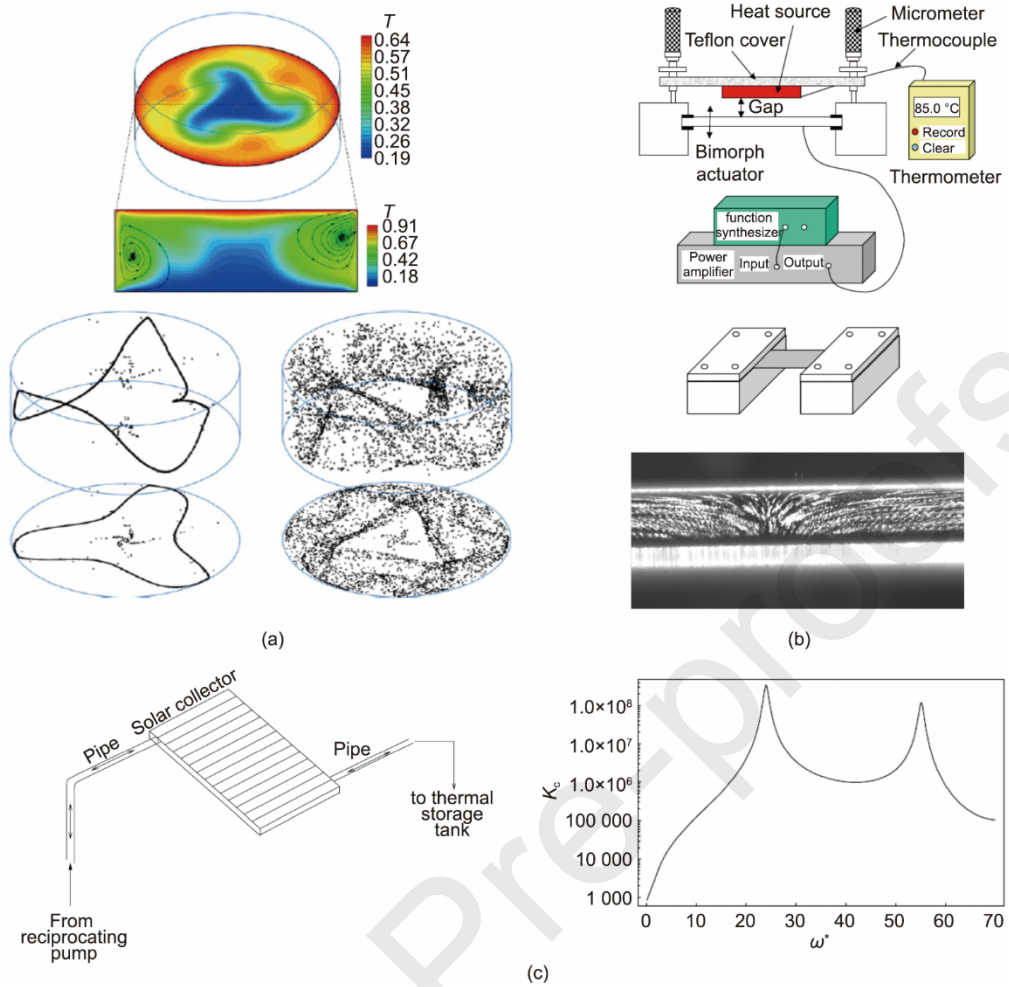

Fig. 13. Coupling of heat transfer with acoustofluidics. (a) evolution of spatial particle distribution in a chamber with a temperature gradient boundary condition [148], (b) Strong streaming introduced at the bottom of an IC chip to control its temperature peak [63], (c) oscillatory flow in a tube enabling an enhanced heat transfer rate [149].

In most of the above studies, the investigators focused on the influence of streaming flow on the enhancement of heat transfer; only a few investigators included the subtle effect of the temperature field itself on the acoustofluidic mechanisms. Recently, a few studies have addressed this subtle coupling between thermal gradients and acoustic waves, revealing what has been called 'baroclinic streaming.' This type of streaming, which sometimes dominates Rayleigh–Schlichting streaming, originates from the temperature dependence of fluid density and compressibility. As explained by Michel and Gissinger [150], this mechanism originates from a nondissipative, purely inviscid process involving strong local gradients of density and compressibility. While many of these recent studies involve excitation in the megahertz domain in microfluidics [151], this effect can be observed with forcing at a few kilohertz in air [150]. In all these studies, baroclinic streaming was found to modify the classical streaming flow, both quantitatively and qualitatively.

4. Discussion and concluding remarks

In this review, the mechanisms, forcing methods, mathematical models, and various applications of acoustofluidics at audible frequencies have been presented and summarized. The current synthesis of the state of the art indicates that the application of audible frequencies imbues streaming flows with unique features, which may be utilized in various applications such as affordable and versatile biological detection, microrobot manipulation, efficient chemical reactors, and many others. The present review aims to provide readers with varying degrees of familiarity with this field with clear insight into the state of the art of both the fundamental and applied aspects of acoustofluidics using audible frequencies.

Low-frequency acoustofluidics has emerged as a valuable technique in various applications and conceptual frameworks as studies have revealed specific advantages compared with acoustofluidics in the ultrasonic range. However, various processes that show promise require further investigation at the level of the underlying mechanisms. Specifically, as mentioned in Section 1.2, certain characteristics are specific to acoustofluidics at audible (and, generally, subultrasonic) frequencies. Several questions that are of critical importance to this topic and have rarely been discussed in previous studies need to be addressed in future studies. Although various studies have been conducted at the applied level, the detailed mechanisms of acoustic streaming remain opaque in certain scenarios, particularly when the forcing amplitude is large.

There are two main aspects that require focused consideration. First, various parameters can influence the magnitude and structure of a streaming flow, notably the local geometry. The particular geometry of microchannels with sharp structures has recently been investigated in a modeling scenario [45], revealing a strong dependence of streaming on the pattern of the structures and their tip angles or curvature diameters [14,46,75,76,89]. This suggests that the influence of geometry might be prevalent in various other scenarios, including classical Kundt tubes and immersed vibrating objects. In the latter case, the use of vibrating spheroids instead of spheres or cylinders has resulted in drift and asymmetry of the vortex locations. More recently, an experimental and analytical investigation of steady streaming around a pair of cylinders was conducted with an exhaustive identification of flow regimes [152], whereas an analytical and numerical study investigated streaming in a linear array of cylinders [153].

In the former case, the influence of a finite width was investigated numerically [134] and was found to be crucial when the channel or tube width was comparable to or smaller than the size of the outer Rayleigh vortices. Therefore, future studies are required to extract and highlight critical geometrical parameters and to integrate these parameters into more reliable models. In this regard, the extensive use of numerical simulations should be beneficial. In the realm of vibrating bubble-induced streaming, the geometry (that is, the shape of the bubble) has recently been shown to be influential [154] because the Minnaert resonance frequency of polyhedral bubbles in the audible range depends on the number of faces of the polygon.

Second, the relatively low frequencies associated with the audible domain, the forcing amplitude may be sufficiently strong for the streaming flow to be of the same order of magnitude as the forcing. Therefore, nontrivial coupling between steady streaming and time-periodic flow may lead to complex advective processes via the nonlinear terms in Eq. (7) and (8) [14,55]: Therefore, classical PT may only provide semi-quantitative predictions in many study environments, thus preventing the determination of the optimal conditions for most of the aforementioned applications. In this respect, the systematic application of the full N–S simulations may be necessary, especially because such an approach remains affordable in terms of computational time and power owing to the relatively large thickness of the VBL where the streaming originates.

Additionally, although a low-frequency acoustic wave (where $\lambda \gg L,\omega$) cannot propagate along the fluid, it can display complex spatial behavior because geometric obstacles can act as diffusers of the wave, even if they may not be considered as sharp (compared to the VBL thickness δ) in the strictest sense. Consequently, in uneven geometries, the spatial structure of the wave may be inhomogeneous, making it difficult to focus the wave action on any local area. The current fabrication of audible-frequency acoustofluidic chips relies on the experimenter's experience. Consequently, several changes of the transducer positions (and the accompanying attachments to the chip with coupling gels or resists) may be required. Improving the integration of a low-frequency transducer and designing the entire packaging with channel and fluid domains remain crucial challenges for future developments in this field. Zhou et al. introduced a high-resolution vibration stage to control the vibration magnitude of a fluid [155]; however, its high cost and relatively complex support equipment might not be conducive to affordable and user-friendly applications, especially those intended for POCT devices.

The topic of acoustofluidics in complex fluids has not been adequately investigated to date. Polymer solutions often exhibit viscoelastic behavior, with a crossover between short-term elastic

behavior and long-term viscous behavior generally occurring at frequencies in the audible range or below [156]. Therefore, actuation should enable the generation of normal stress, a mechanism that has been invoked to thicken the VBL or induce flow reversal in experiments on vibrating immersed cylinders by Böohme [157] and Chang et al. [158]. More recently, Vishwanathan and Juarez observed flow distortion and a non-monotonic dependence on frequency in Maxwell-type fluids [159]. Furthermore, the possibility of achieving large strain forcing at audible frequencies could enable better mixing and homogenization of yield stress (or elastoviscoplastic) fluids. For typical yield-stress fluids, the typical time scale for inducing the solid–liquid transition also corresponds to the range of audible frequencies (and below) [160,161]; consequently, periodic actuation of such complex fluids is also a promising topic for further investigation.

Finally, very few studies have investigated the effects of nonharmonic forcing on streaming. A classic example was proposed by Tatsuno [162], who emphasized a variety of promising methods for inducing uneven flows accompanied by pathways for further enhancing mixing. To advance our understanding of this topic, the application of more complex forcing, for instance with frequency or amplitude modulation, or forcing that includes a proportion of noise, could be a valuable subject for future investigations. In this respect, the ability to harvest nonharmonic broadband vibrations (inherent in many industrial processes) to generate complex streaming flows could be especially insightful.

Acknowledgments

This project was financially supported by the National Key R&D Program of China (2022YFC2406600 and 2020YFB2009000) and the Program for Innovation Team of Shaanxi Province (2021TD-23). All authors extend their heartfelt gratitude to Professor John Lomas from Université Paris Cité for his invaluable assistance in refining this paper and improving its linguistic quality.

Compliance with ethics guidelines

Chuanyu Zhang, Philippe Brunet, Shuo Liu, Xiaofeng Guo, Laurent Royon, Xianming Qin, and Xueyong Wei declare that they have no conflict of interest or financial conflicts to disclose.

References

[1] Kundt A. Ueber eine neue art akustischer staubfiguren und über die anwendung derselben zur bestimmung der schallgeschwindigkeit in festen körpern und gasen. Ann Phys 1866;203(4):497–523.

[2] Yasuda K, Umemura SI, Takeda K. Concentration and fractionation of small particles in liquid by ultrasound. Jpn J Appl Phys 1995;34(5S):2715–20.

[3] Faraday M. XVII. On a peculiar class of acoustical figures; and on certain forms assumed by groups of particles upon vibrating elastic surfaces. Phil Trans R Soc 1831;121:299–340.

[4] Nyborg WL. Acoustic streaming due to attenuated plane waves. J Acoust Soc Am 1953;25(1):68–75.

[5] Nyborg WL. Acoustic streaming near a boundary. J Acoust Soc Am 1958;30(4):329–39.

[6] Lighthill J. Acoustic Streaming. J Sound Vibrat 1978;61(3):391–418.

[7] Trinh EH, Gopinath A. Acoustic streaming and heat and mass transfer enhancement. In: Proceedings of the Third Microgravity Fluid Physics Conference; 1996 Jul 13–15; Cleveland, OH, USA. NASA; 1996. p. 791–6.

[8] Johnson DA, Feke DL. Methodology for fractionating suspended particles using ultrasonic standing wave and divided flow fields. Sep Technol 1995;5(4):251–8.

[9] Rousseaux G, Yoshikawa H, Stegner A, Wesfreid JE. Dynamics of transient eddy above rolling-grain ripples. Phys Fluids 2004;16(4):1049–58.

[10] Bahrani SA, P'erinet N, Costalonga M, Royon L, Brunet P. Vortex elongation in outer streaming flows. Exp Fluids 2020;61:91.

[11] Data Physicalization. List of Physical Visualizations/kundts-tube. Report. Dagstuhl: Data Physicalization. 2012.

[12] Data Physicalization. List of Physical Visualizations/Chladni Plates. Report. Dagstuhl: Data Physicalization. 2012.

[13] Vukasinovic B, Smith MK, Glezer A. Dynamics of a sessile drop in forced vibration. J Fluid Mech 2007;587:395–423.

[14] Zhang C, Guo X, Brunet P, Costalonga M, Royon L. Acoustic streaming near a sharp structure and its mixing performance characterization. Microfluid Nanofluid 2019;23:104.

[15] Wang, C., Jalikop, S. V. & Hilgenfeldt, S. Efficient manipulation of microparticles in bubble streaming flows. Biomicrofluidics 2012; 6(1): 012801

[16] Dong Z, Yao C, Zhang X, Xu J, Chen G, Zhao Y, et al. A high-power ultrasonic microreactor and its application in gas-liquid mass transfer intensification. Lab Chip 2015;15(4):1145–52.

[17] Bahrani SA, Herbaut R, Royon L, Azzouz K, Bontemps A. Experimental investigation of thermal and flow mixing enhancement induced by Rayleigh-like streaming in a milli-mixer. Therm Sci Eng Prog 2019;14:100434.

[18] H. Bruus. Acoustofluidics 2: Perturbation theory and ultrasound resonance modes. Lab Chip 2012;12:20–8:.

[19] Xie Y, Mao Z, Bachman H, Li P, Zhang P, Ren L, et al. Acoustic cell separation based on density and mechanical properties. J Biomech Eng 2020;142(3):031005.

[20] Qin X, Wei X, Li L, Wang H, Jiang Z, Sun D. Acoustic valves in microfluidic channels for droplet manipulation. Lab Chip 2021;21(16):3165–73.

[21] He S, Wang Z, Pang W, Liu C, Zhang M, Yang Y, et al. Ultra-rapid modulation of neurite outgrowth in a gigahertz acoustic streaming system. Lab Chip 2021;21(10):1948–55.

[22] Blondeaux P. Sand ripples under sea waves Part 1. Ripple formation. J Fluid Mech 1990;218:1–17.

[23] Yang Y, Zhang L, Jin K, He M, Wei W, Chen X, et al. Self-adaptive virtual microchannel for continuous enrichment and separation of nanoparticles. Sci Adv 2022;8(30):eabn8440.

[24] Dvořák V. Ueber die entstehungsweise der kundt'schen staubfiguren. Ann Phys 1874;227(4):634–9.

[25] Andrade ENC, Filon LNG. On the circulations caused by the vibration of air in a tube. Proc R Soc A 1931;134(824):445–70.

[26] Holtsmark J, Johnsen I, Sikkeland T, Skavlem S. Boundary layer flow near a cylindrical obstacle in an oscillating, incompressible fluid. J Acoust Soc Am 1954;26(1):26–39.

[27] Wang CY. On high-frequency oscillatory viscous flows. J Fluid Mech 1968;32(1):55–68.

[28] Stuart JT. Double boundary layers in oscillatory viscous flow. J Fluid Mech 1966;24(4):673–87.

[29] Tatsuno M. Circulatory streaming around an oscillating circular cylinder at low Reynolds numbers. J Phys Soc Jpn 1973;35(3):915–20.

[30] Tatsuno M, Bearman PW. A visual study of the flow around an oscillating circular cylinder at low Keulegan–Carpenter numbers and low Stokes numbers. J Fluid Mech 1990;211:157–82.

[31] Riley N. Oscillating viscous flows. Mathematika 1965;12(2):161–75.

[32] Riley N. Steady streaming. Annu Rev Fluid Mech 2001;33:43–65.

[33] Boluriaan S, Morris PJ. Acoustic streaming: from Rayleigh to today. Int J Aeroacoust 2003;2(3):255–92.

[34] Costalonga M, Brunet P, Peerhossaini H. Low frequency vibration induced streaming in a Hele-Shaw cell. Phys Fluids 2015;27(1):013101.

[35] Xu R, Akay H, Kim SG. Buckled MEMS beams for energy harvesting from low frequency vibrations. Research 2019;2019:1087946.

[36] Ingård U, Labate S. Acoustic circulation effects and the nonlinear impedance of orifices. J Acoust Soc Am 1950;22(2):211–8.

[37] Lebedeva IV. Experimental study of acoustic streaming in the vicinity of orifices. Sov Phys Acoust 1980;26:331–3.

[38] James RD, Jacobs JW, Glezer A. A round turbulent jet produced by an oscillating diaphragm. Phys Fluids 1996;8(9):2484–95.

[39] Gimeno L, Talbi A, Viard R, Merlen A, Pernod P, Preobrazhensky V. Synthetic jets based on micro magneto mechanical systems for aerodynamic flow control. J Micromech Microeng 2010;20(7):075004.

[40] Longuet-Higgins MS. Mass transport in water waves. Philos Trans R Soc A 1953;245(903):535–81.

[41] Cinbis C, Mansour NN, Khuri-Yakub BT. Effect of surface tension on the acoustic radiation pressure-induced motion of the water–air interface. J Acoust Soc Am 1993;94(4):2365–72.

[42] Simon JC, Sapozhnikov OA, Khokhlova VA, Crum LA, Bailey MR. Ultrasonic atomization of liquids in drop-chain acoustic fountains. J Fluid Mech 2015;766:129–46.

[43] Brunet P, Eggers J, Deegan RD. Vibration-induced climbing of drops. Phys Rev Lett 2007;99(14):144501.

[44] Costalonga M, Brunet P. Directional motion of vibrated sessile drops: a quantitative study. Phys Rev Fluids 2020;5(2):023601.

[45] Ovchinnikov M, Zhou J, Yalamanchili S. Acoustic streaming of a sharp edge. J Acoust Soc Am 2014;136(1):22–9.

[46] Huang PH, Xie Y, Ahmed D, Rufo J, Nama N, Chen Y, et al. An acoustofluidic micromixer based on oscillating sidewall sharp-edges. Lab Chip 2013;13(19):3847–52.

[47] Zhang P, Bachman H, Ozcelik A, Huang TJ. Acoustic microfluidics. Annu Rev Anal Chem 2020;13:17–43.

[48] Wu M, Ozcelik A, Rufo J, Wang Z, Fang R, Huang TJ. Acoustofluidic separation of cells and particles. Microsyst Nanoeng 2019;5:32.

[49] Friend J, Yeo LY. Microscale acoustofluidics: microfluidics driven via acoustics and ultrasonics. Rev Mod Phys 2011;83(2):647–704.

[50] Chladni EFF. Entdeckungen über die theorie des klanges. Leipzig: Weidmanns Erben und Reich; 1787.

[51] Bruus H. Acoustofluidics 1: governing equations in microfluidics. Lab Chip 2011;11(22):3742–51.

[52] Ding X, Li P, Lin SCS, Stratton ZS, Nama N, Guo F, et al. Surface acoustic wave microfluidics. Lab Chip 2013;13(18):3626–49.

[53] Ozcelik A, Rufo J, Guo F, Gu Y, Li P, Lata J, et al. Acoustic tweezers for the life sciences. Nat Methods 2018;15(12):1021–8.

[54] Hamilton MF, Ilinskii YA, Zabolotskaya EA. Thermal effects on acoustic streaming in standing waves. J Acoust Soc Am 2003;114(6):3092–101.

[55] Zhong G, Liu Y, Guo X, Royon L, Brunet P. Vibration-induced streaming flow near a sharp edge: Flow structure and instabilities in a large span of forcing amplitude. Phys Rev E 2023;107(2):025102.

[56] Tian C, Liu W, Zhao R, Li T, Xu J, Chen SW, et al. Acoustofluidics-based enzymatic constant determination by rapid and stable in situ mixing. Sens Actuators B Chem 2018;272:494–501.

[57] Wang S, Huang X, Yang C. Microfluidic bubble generation by acoustic field for mixing enhancement. J Heat Transfer 2012;134(5):051014.

[58] Marmottant P, Hilgenfedlt S. Controlled vesicle deformation and lysis by single oscillating bubbles. Nature 2003;423(6936):153–6.

[59] Hao N, Liu P, Bachman H, Pei Z, Zhang P, Rufo J, et al. Acoustofluidics-assisted engineering of multifunctional three-dimensional zinc oxide nanoarrays. ACS Nano 2020;14(5):6150–63.

[60] Huang PH, Zhao S, Bachman H, Nama N, Li Z, Chen C, et al. Acoustofluidic synthesis of particulate nanomaterials. Adv Sci 2019;6(19):1900913.

[61] Liu RH, Yang J, Pindera MZ, Athavale M, Grodzinski P. Bubble-induced acoustic micromixing. Lab Chip 2002;2(3):151–7.

[62] Surendran V, Chiulli T, Manoharan S, Knisley S, Packirisamy M, Chandrasekaran A. Acoustofluidic micromixing enabled hybrid integrated colorimetric sensing, for rapid point-of-care measurement of salivary potassium. Biosensors 2019;9(2):73.

[63] Wu T, Ro PI. Heat transfer performance of a cooling system using vibrating piezoelectric beams. J Micromech Microeng 2005;15(1):213–20.

[64] Park JH, Bae KT, Kim KJ, Joh DW, Kim D, Myung J, et al. Ultra-fast fabrication of tape-cast anode supports for solid oxide fuel cells via resonant acoustic mixing technology. Ceram Int 2019;45(9):12154–61.

[65] Chindam C, Nama N, Ian Lapsley M, Costanzo F, Jun Huang T. Theory and experiment on resonant frequencies of liquid-air interfaces trapped in microfluidic devices. J Appl Phys 2013;114(19):194503.

[66] Bachman H, Gu Y, Rufo J, Yang S, Tian Z, Huang PH, et al. Low-frequency flexural wave based microparticle manipulation. Lab Chip 2020;20(7):1281–9.

[67] Liu X, Shi Q, Lin Y, Kojima M, Mae Y, Fukuda T, et al. Multifunctional noncontact micromanipulation using whirling flow generated by vibrating a single piezo actuator. Small 2019;15(5):1804421.

[68] Durrer J, Agrawal P, Ozgul A, Neuhauss SCF, Nama N, Ahmed D. A robot-assisted acoustofluidic end effector. Nat Commun 2022;13:6370.

[69] Marmottant P, Hilgenfeldt S. A bubble-driven microfluidic transport element for bioengineering. Proc Natl Acad Sci USA 2004;101(26):9523–7.

[70] Ahmed D, Mao X, Shi J, Juluri BK, Huang TJ. A millisecond micromixer via single-bubble-based acoustic streaming. Lab Chip 2009;9(18):2738–41.

[71] Ahmed D, Mao X, Juluri BK, Huang TJ. A fast microfluidic mixer based on acoustically driven sidewall-trapped microbubbles. Microfluid Nanofluid 2009;7:727–31.

[72] Kotas CW, Yoda M, Rogers PH. Visualization of steady streaming near oscillating spheroids. Exp Fluids 2007;42:111–21.

[73] Wiklund M, Green R, Ohlin M. Acoustofluidics 14: applications of acoustic streaming in microfluidic devices. Lab Chip 2012;12(14):2438–51.

[74] Muller PB, Rossi M, Marín ÁG, Barnkob R, Augustsson P, Laurell T, et al. Ultrasound-induced acoustophoretic motion of microparticles in three dimensions. Phys Rev E 2013;88(2):023006.

[75] Nama N, Huang PH, Huang TJ, Costanzo F. Investigation of acoustic streaming patterns around oscillating sharp edges. Lab Chip 2014;14(15):2824–36.

[76] Zhang C, Guo X, Royon L, Brunet P. Unveiling of the mechanisms of acoustic streaming induced by sharp edges. Phys Rev E 2020;102(4):043110.

[77] Zhang C, Guo X, Royon L, Brunet P. Acoustic streaming generated by sharp edges: the coupled influences of liquid viscosity and acoustic frequency. Micromachines (Basel) 2020;11(6):607.

[78] Lieu VH, House TA, Schwartz DT. Hydrodynamic tweezers: impact of design geometry on flow and microparticle trapping. Anal Chem 2012;84(4):1963–8.

[79] Lee CP, Wang TG. Near-boundary streaming around a small sphere due to two orthogonal standing waves. J Acoust Soc Am 1989;85(3):1081–8.

[80] Lei, J.; Glynne-Jones, P.; Hill, M. Comparing Methods for the Modelling of Boundary-Driven Streaming in Acoustofluidic Devices. Microfluid. Nanofluidics 2017, 21 (2), 1–11.

[81] Orosco J, Friend J. Modeling fast acoustic streaming: steady-state and transient flow solutions. Phys Rev E 2022;106(4):045101.

[82] Makarov SN, Semenova NG, Smirnov VE. Acoustic streaming model for an intense sound beam in free space. Fluid Dyn 1989;24(6):823–6.

[83] Moudjed B, Botton V, Henry D, Ben Hadid H, Garandet JP. Scaling and dimensional analysis of acoustic streaming jets. Phys Fluids 2014;26(9):093602.

[84] Frenkel V, Gurka R, Liberzon A, Shavit U, Kimmel E. Preliminary investigations of ultrasound induced acoustic streaming using particle image velocimetry. Ultrasonics 2001;39(3):153–6.

[85] Mitome H. The mechanism of generation of acoustic streaming. Electron Commun Jpn Part III 1998;81(10):1–8.

[86] Kamakura T, Sudo T, Matsuda K, Kumamoto Y. Time evolution of acoustic streaming from a planar ultrasound source. J Acoust Soc Am 1996;100(1):132–8.

[87] Dentry MB, Yeo LY, Friend JR. Frequency effects on the scale and behavior of acoustic streaming. Phys Rev E 2014;89(1):013203.

[88] Huang PH, Nama N, Mao Z, Li P, Rufo J, Chen Y, et al. A reliable and programmable acoustofluidic pump powered by oscillating sharp-edge structures. Lab Chip 2014;14(22):4319–23.

[89] Zhang C, Brunet P, Royon L, Guo X. Mixing intensification using sound-driven micromixer with sharp edges. Chem Eng J 2021;410:128252.

[90] Chen H, Chen C, Bai S, Gao Y, Metcalfe G, Cheng W, et al. Multiplexed detection of cancer biomarkers using a microfluidic platform integrating single bead trapping and acoustic mixing techniques. Nanoscale 2018;10(43):20196–206.

[91] Chen H, Gao Y, Petkovic K, Yan S, Best M, Du Y, et al. Reproducible bubble-induced acoustic microstreaming for bead disaggregation and immunoassay in microfluidics. Microfluid Nanofluid 2017;21:30.

[92] Yang C, Yu Y, Zhao Y, Shang L. Bioinspired jellyfish microparticles from microfluidics. Research 2023;6:0034.

[93] Feng L, Song B, Chen Y, Liang S, Dai Y, Zhou Q, et al. On-chip rotational manipulation of microbeads and oocytes using acoustic microstreaming generated by oscillating asymmetrical microstructures. Biomicrofluidics 2019;13(6):064103.

[94] Feng L, Song B, Zhang D, Jiang Y, Arai F. On-chip tunable cell rotation using acoustically oscillating asymmetrical microstructures. Micromachines (Basel) 2018;9(11):596.

[95] Bai X, Song B, Chen Z, Zhang W, Chen D, Dai Y, et al. Postoperative evaluation of tumours based on label-free acoustic separation of circulating tumour cells by microstreaming. Lab Chip 2021;21(14):2721–9.

[96] Huang PH, Ren L, Nama N, Li S, Li P, Yao X, et al. An acoustofluidic sputum liquefier. Lab Chip 2015;15(15):3125–31.

[97] Gao Y, Tran P, Petkovic-Duran K, Swallow T, Zhu Y. Acoustic micromixing increases antibody-antigen binding in immunoassays. Biomed Microdevices 2015;17(4):79.

[98] Liu RH, Yang J, Lenigk R, Bonanno J, Grodzinski P. Self-contained, fully integrated biochip for sample preparation, polymerase chain reaction amplification, and DNA microarray detection. Anal Chem 2004;76(7):1824–31.

[99] Liu RH, Lenigk R, Grodzinski PA. Acoustic micromixer for enhancement of DNA biochip systems. J Micro/Nanolith MEMS MOEMS 2003;2(3):178–84.

[100] Kardous F, Rouleau A, Simon B, Yahiaoui R, Manceau JF, Boireau W. Improving immunosensor performances using an acoustic mixer on droplet microarray. Biosens Bioelectron 2010;26(4):1666–71.

[101] Wang Z, Huang PH, Chen C, Bachman H, Zhao S, Yang S, et al. Cell lysis via acoustically oscillating sharp edges. Lab Chip 2019;19(24):4021–32.

[102] Zhao S, He W, Ma Z, Liu P, Huang PH, Bachman H, et al. On-chip stool liquefaction via acoustofluidics. Lab Chip 2019;19(6):941–7.

[103] Ahmed D, Ozcelik A, Bojanala N, Nama N, Upadhyay A, Chen Y, et al. Rotational manipulation of single cells and organisms using acoustic waves. Nat Commun 2016;7:11085.

[104]Läubli NF, Shamsudhin N, Vogler H, Munglani G, Grossniklaus U, Ahmed D, et al. 3D manipulation and imaging of plant cells using acoustically activated microbubbles. Small Methods 2019;3(3):1800527.

[105] Läubli NF, Gerlt MS, Wüthrich A, Lewis RTM, Shamsudhin N, Kutay U, et al. Embedded microbubbles for acoustic manipulation of single cells and microfluidic applications. Anal Chem 2021;93(28):9760–70.

[106]Chung SK, Cho SK. On-chip manipulation of objects using mobile oscillating bubbles. J Micromech Microeng 2008;18(12):125024.

[107]Chung SK, Cho SK. 3-D manipulation of millimeter- and micro-sized objects using an acoustically excited oscillating bubble. Microfluid Nanofluid 2009;6(2):261–5.

[108]Liu X, Shi Q, Lin Y, Kojima M, Mae Y, Huang Q, et al. Hydrodynamic tweezers: trapping and transportation in microscale using vortex induced by oscillation of a single piezoelectric actuator. Sensors (Basel) 2018;18(7):2002.

[109]Lutz BR, Chen J, Schwartz DT. Hydrodynamic tweezers: 1. noncontact trapping of single cells using steady streaming microeddies. Anal Chem 2006;78(15):5429–35.

[110]Bai X, Bin S, Yuguo D, Wei Z, Yanmin F, Yuanyuan C, et al. Parallel trapping, patterning, separating and rotating of micro-objects with various sizes and shapes using acoustic microstreaming. Sens Actuators A Phys 2020;315:112340.

[111]Hayakawa T, Sakuma S, Arai F. On-chip 3D rotation of oocyte based on a vibration-induced local whirling flow. Microsyst Nanoeng 2015;1:15001.

[112]Hayaawa T, Sakuma S, Fukuhara T, Yokoyama Y, Arai F. A single cell extraction chip using vibration-induced whirling flow and a thermo-responsive gel pattern. Micromachines (Basel) 2014;5(3):681–96.

[113]Hayakawa T, Arai F. On-chip micromanipulation method based on mode switching of vibration-induced asymmetric flow. In: Proceedings of the International Conference on Robotics and Automation (ICRA); 2017 May 29–Jun 3; Singapore. IEEE; 2017. p. 6631–6.

[114] Moshksayan K, Kashaninejad N, Warkiani ME, Lock JG, Moghadas H, Firoozabadi B, et al. Spheroids-on-a-chip: recent advances and design considerations in microfluidic platforms for spheroid formation and culture. Sens Actuators B Chem 2018;263:151–76.

[115] Shao C, Chi J, Zhang H, Fan Q, Zhao Y, Ye F. Development of cell spheroids by advanced technologies. Adv Mater Technol 2020;5(9):2000183.

[116] Ozcelik A, Nama N, Huang PH, Kaynak M, McReynolds MR, Hanna-Rose W, et al. Acoustofluidic rotational manipulation of cells and organisms using oscillating solid structures. Small 2016;12(37):5120–5.

[117]Rasouli R, Tabrizian M. Rapid formation of multicellular spheroids in boundary-driven acoustic microstreams. Small 2021;17(39):2101931.

[118]Gao Y, Wu M, Luan Q, Papautsky I, Xu J. Acoustic bubble for spheroid trapping, rotation, and culture: a tumor-on-a-chip platform (ABSTRACT platform). Lab Chip 2022;22(4):805–13.

[119] Wang S, Huang X, Yang C. Mixing enhancement for high viscous fluids in a microfluidic chamber. Lab Chip 2011;11(12):2081–7.

[120]Nama N, Huang PH, Huang TJ, Costanzo F. Investigation of micromixing by acoustically oscillated sharp-edges. Biomicrofluidics 2016;10(2):024124.

[121]Hao N, Pei Z, Liu P, Bachman H, Naquin TD, Zhang P, et al. Acoustofluidics-assisted fluorescence-SERS bimodal biosensors. Small 2020;16(48):2005179.

[122]Zhao X, Chen H, Xiao Y, Zhang J, Qiu Y, Wei J, et al. Rational design of robust flower-like sharp-edge acoustic micromixers towards efficient engineering of functional 3D ZnO nanorod array. Chem Eng J 2022;447:137547.

[123]Chen Z, Pei Z, Zhao X, Zhang J, Wei J, Hao N. Acoustic microreactors for chemical engineering. Chem Eng J 2022;433(Pt 2):133258.

[124]Tang SY, Ayan B, Nama N, Bian Y, Lata JP, Guo X, et al. On-chip production of size-controllable liquid metal microdroplets using acoustic waves. Small 2016;12(28):3861–9.

[125]Ahmed D, Muddana HS, Lu M, French JB, Ozcelik A, Fang Y, et al. Acoustofluidic chemical waveform generator and switch. Anal Chem 2014;86(23):11803–10.

[126] Xie Y, Chindam C, Nama N, Yang S, Lu M, Zhao Y, et al. Exploring bubble oscillation and mass transfer enhancement in acoustic-assisted liquid-liquid extraction with a microfluidic device. Sci Rep 2015;5:12572.

[127]Fung K, Li Y, Fan S, Fajrial AK, Ding Y, Ding X. Acoustically excited microstructure for on-demand fouling mitigation in a microfluidic membrane filtration device. J Membr Sci Lett 2022;2(1):100012.

[128] Dijkink RJ, Van Der Dennen JP, Ohl CD, Prosperetti A. The 'acoustic scallop': a bubble-powered actuator. J Micromech Microeng 2006;16(8):1653–9.

[129]Feng J, Yuan J, Cho SK. Micropropulsion by an acoustic bubble for navigating microfluidic spaces. Lab Chip 2015;15(6):1554–62.

[130]Ryu K, Chung SK, Cho SK. Micropumping by an acoustically excited oscillating bubble for automated implantable microfluidic devices. J Assoc Lab Autom 2010;15(3):163–71.

[131]Ryu K, Zueger J, Chung SK, Cho SK. Underwater propulsion using AC-electrowetting-actuated oscillating bubbles for swimming robots. In: Proceedings of the 23rd International Conference on Micro Electro Mechanical Systems (MEMS); 2010 Jan 24–28; Hong Kong, China. IEEE; 2010. p. 160–3.

[132]Tovar AR, Patel MV, Lee AP. Lateral air cavities for microfluidic pumping with the use of acoustic energy. Microfluid Nanofluid 2011;10(6):1269–78.

[133] Tovar AR, Lee AP. Lateral cavity acoustic transducer. Lab Chip 2009;9(1):41–3.

[134]Hamilton MF, Ilinskii YA, Zabolotskaya EA. Acoustic streaming generated by standing waves in two-dimensional channels of arbitrary width. J Acoust Soc Am 2003;113(1):153–60.

[135]Mozurkewich G. Heat transfer from a cylinder in an acoustic standing wave. J Acoust Soc Am 1995;98(4):2209–16.

[136]Mozurkewich G. Heat transfer from transverse tubes adjacent to a thermoacoustic stack. J Acoust Soc Am 2001;110(2):841–7.

[137]Mozurkewich G. Heat transport by acoustic streaming within a cylindrical resonator. Appl Acoust 2002;63(7):713–35.

[138]Gopinath A. Convective heat transfer in acoustic streaming flows [dissertation]. Los Angeles: University of California at Los Angeles; 1992.

[139] Gopinath A, Mills AF. Convective heat transfer due to acoustic streaming across the ends of a Kundt tube. J Heat Transfer 1994;116(1):47–53.

[140] Gopinath A, Harder DR. An experimental study of heat transfer from a cylinder in low-amplitude zero-mean oscillatory flows. Int J Heat Mass Transfer 2000;43(4):505–20.

[141]Gopinath A, Mills AF. Convective heat transfer from a sphere due to acoustic streaming. J Heat Transfer 1993;115(2):332–41.

[142]Kamotani Y, Prasad A, Ostrach S. Thermal convection in an enclosure due to vibrations aboard spacecraft. AIAA J 1981;19(4):511–6.

[143] Farooq A, Homsy GM. Streaming flows due to g-jitter-induced natural convection. J Fluid Mech 1994;271(2):351–78.

[144] Hirata K, Tatsumoto K, Nobuhara M, Tanigawa H. On g-jitter effects on three-dimensional laminar thermal convection in low gravity. Mech Eng J 2015;2(5):15-00268.

[145] Hirata K, Nobuhara M, Kodama M, Tanigawa H, Noguchi T. Three-pronged convection in a cubic cavity under modulating gravity. Int J Heat Mass Transfer 2019;135:1073–81.

[146] Tatsumoto K, Nobuhara M, Tanigawa H, Hirata K. Thermal convection inside an oscillating cube analysed with proper orthogonal decomposition. Mech Eng J 2015;2(2):15-00018.

[147] Dyko MP, Vafai K. Effects of gravity modulation on convection in a horizontal annulus. Int J Heat Mass Transfer 2007;50(1–2):348–60.

[148]Lappa M. On the variety of particle accumulation structures under the effect of g-jitters. J Fluid Mech 2013;726:160–95.

[149]Lambert AA, Cuevas S, del Río JA. Enhanced heat transfer using oscillatory flows in solar collectors. Sol Energy 2006;80(10):1296–302.

[150]Michel G, Gissinger C. Cooling by baroclinic acoustic streaming. Phys Rev Appl 2021;16(5):L051003.

[151]Joergensen JH, Qiu W, Bruus H. Transition from boundary-driven to bulk-driven acoustic streaming due to nonlinear thermoviscous effects at high acoustic energy densities. Phys Rev Lett 2023;130(4):044001.

[152]Coenen W. Steady streaming around a cylinder pair. Proc R Soc A 2016;472(2195):20160522.

[153] Alaminos-Quesada J, Lawrence JJ, Coenen W, Sánchez AL. Oscillating viscous flow past a streamwise linear array of circular cylinders. J Fluid Mech 2023;959:A39.

[154]Boughzala M, Stephan O, Bossy E, Dollet B, Marmottant P. Polyhedral bubble vibrations. Phys Rev Lett 2021;126(5):054502.

[155] Zhou Y, Wang H, Ma Z, Yang JKW, Ai Y. Acoustic vibration-induced actuation of multiple microrotors in microfluidics. Adv Mater Technol 2020;5(9):2000323.

[156]Joseph DD. Fluid dynamics of viscoelastic liquids. Berlin: Springer; 1990.

[157]Böhme G. On steady streaming in viscoelastic liquids. J Non-Newt Fluid Mech 1992;44:149–70.

[158]Chang CF, Schowalter W. Secondary flow in the neighborhood of a cylinder oscillating in a viscoelastic fluid. J Non-Newt Fluid Mech 1979;6(1):47–67.

[159]Vishwanathan G, Juarez G. Steady streaming flows in viscoelastic liquids. J Non-Newt Fluid Mech 2019;271:104143.

[160] Benmouffok-Benbelkacem G, Caton F, Baravian C, Skali-Lami S. Non-linear viscoelasticity and temporal behavior of typical yield stress fluids: Carbopol, Xanthan and Ketchup. Rheol Acta 2010;49(3):305–14.

[161]Varchanis S, Haward SJ, Hopkins CC, Syrakos A, Shen AQ, Dimakopoulos Y, et al. Transition between solid and liquid state of yield-stress fluids under purely extensional deformations. Proc Natl Acad Sci USA 2020;117(23):12611–7.

[162]Tatsuno M. Secondary flow induced by a circular cylinder performing unharmonic oscillations. J Phys Soc Jpn 1981;50(1):330–7.

Declaration of interests

☒ The authors declare that they have no known competing financial interests or personal relationships that could have appeared to influence the work reported in this paper.

☐The authors declare the following financial interests/personal relationships which may be considered as potential competing interests: